

# Towards the theory of coherent hard dijet production on hadrons and nuclei

V.M. BRAUN<sup>1</sup>, D.YU. IVANOV<sup>1,2</sup> A. SCHÄFER<sup>1</sup> and L. SZYMANOWSKI<sup>3,4</sup>

<sup>1</sup>*Institut für Theoretische Physik, Universität Regensburg,  
D-93040 Regensburg, Germany*

<sup>2</sup>*Institute of Mathematics, 630090 Novosibirsk, Russia*

<sup>3</sup>*CPhT, École Polytechnique, F-91128 Palaiseau, France\**

<sup>4</sup>*Soltan Institute for Nuclear Studies, Hoza 69,  
00-681 Warsaw, Poland*

*October 31, 2018*

## Abstract:

We carry out a detailed calculation of the cross section of pion diffraction dissociation into two jets with large transverse momenta, originating from a hard gluon exchange between the pion constituents. Both the quark and the gluon contribution are considered and in the latter case we present calculations both in covariant and in axial gauges. We find that the standard collinear factorization does not hold in this reaction. The structure of non-factorizable contributions is discussed and the results are compared with the experimental data. Our conclusion is that the existing theoretical uncertainties do not allow, for the time being, for a quantitative extraction of the pion distribution amplitude.

*Submitted to Nuclear Physics B*

---

\*Unité mixte C7644 du CNRS.

# Contents

<b>1</b>	<b>Introduction</b>	<b>2</b>
<b>2</b>	<b>The Quark Contribution</b>	<b>5</b>
2.1	The Calculation . . . . .	5
2.2	The End-Point Behavior . . . . .	9
<b>3</b>	<b>Gluon Contribution</b>	<b>12</b>
3.1	Getting Started: Exclusive Vector Meson Production . . . . .	12
3.2	Dijet production: Dispersion approach . . . . .	18
3.3	Dijet production: Factorization and the light-cone limit . . . . .	23
3.4	Discussion . . . . .	30
<b>4</b>	<b>Numerical Analysis</b>	<b>31</b>
<b>5</b>	<b>Conclusions</b>	<b>36</b>
<b>A</b>	<b>Generalized parton distributions in symmetric notation</b>	<b>38</b>
<b>B</b>	<b>Summary of Results</b>	<b>39</b>
	<b>References</b>	<b>43</b>

# 1 Introduction

After thirty years of Quantum Chromodynamics, many aspects of hadron structure remain poorly understood. The bulk of the existing experimental information comes from parton distributions that can be interpreted as one-particle probabilities to find quarks, antiquarks and gluons carrying certain momentum fractions of the parent hadron. The parton distributions are inclusive quantities, in the sense that contributions of different parton states are summed over, and therefore provide us only with global information about the hadron wave function. It is well known that hard exclusive reactions allow, in principle, to separate contributions of different Fock states and study the momentum fraction distributions of the components with the minimum number of Fock constituents at small transverse separations, dubbed distribution amplitudes. In practice, however, progress in this direction had been limited, due to both experimental difficulties to isolate exclusive amplitudes and theoretical problems to formulate their quantitative description.

Classical applications of QCD to exclusive reactions addressed electromagnetic form factors [1, 2, 3]. Nowadays it is almost generally accepted, however, that the asymptotic behavior of form factors is only achieved for very large momentum transfers. In addition, the form factors involve a convolution (overlap integral) of distribution amplitudes which makes it difficult to extract them directly from the data. In recent years, the list of applications of QCD factorization to hard exclusive reactions have been increased significantly, with hard exclusive meson production [8, 4] and deeply-virtual Compton scattering (DVCS) [5, 6, 7] providing notable examples. This raises hopes that suitable hard processes can be found in which hadron distribution amplitudes can be studied in a more direct way.

In particular, coherent diffractive production of dijets by incident pions (or photons) on nuclei has attracted a lot of attention. The subject of diffraction is very old. Ever since the classic works in early 50' on the diffraction breakup of deuterons [9] it was known that the momentum distribution of the proton and the neutron in the final state is close to their momentum distribution as deuteron constituents. More recently, the same idea gave rise to the method of so-called Coulomb Explosion Imaging [10] which is widely used to study the high-momentum tails of wave functions of small molecules. To our knowledge, the pion (and photon) diffraction dissociation into a pair of jets with large transverse momentum on a nucleon target was first discussed in [11]. In Ref. [12] the possibility to use this process to probe the nuclear filtering of pion components with a small transverse size was suggested. The  $A$ -dependence and the  $q_\perp^2$ -dependence of the coherent dijet cross section was first calculated in [13]. In the same work it was argued that the jet distribution with respect to the longitudinal momentum fraction has to follow the quark momentum distribution in the pion and hence provides a direct measurement of the pion distribution amplitude. Recent experimental data by the E791 collaboration [14, 15] indeed confirm the strong  $A$ -dependence which is a signature for color transparency, and are consistent with the predicted  $\sim 1/q_\perp^8$  dependence on the jet transverse momentum. Moreover, the jet longitudinal momentum fraction distribution turns out to be consistent with the  $\sim z^2(1-z)^2$  shape corresponding to the asymptotic pion distribution amplitude which is also supported by an independent measurement of the pion transition form factor

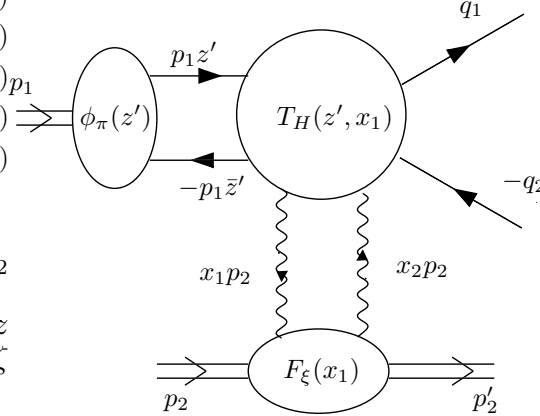


Figure 1: Kinematics of the coherent hard dijet production  $\pi \rightarrow 2$  jets. The hard scattering amplitude  $T_H$  contains at least one hard gluon exchange.

$\pi\gamma\gamma^*$  [16].

After these first successes, one naturally asks whether the QCD description of coherent dijet production can be made fully quantitative. Two recent papers [17] and [18] address this question, with contradictory conclusions. In the present work we attempt to clarify the situation and develop a perturbative QCD framework for the description of coherent dijet production that would be in line with other known applications of the QCD factorization techniques. Some of the results reported in this paper were published earlier in a letter format [19]. An approach close to ours was suggested independently in [20], [21]. We disagree with [20, 21] on several important issues and the reasons for this disagreement will be elucidated in what follows.

The kinematics of the process is shown in Fig. 1. For definiteness, we consider  $\pi^-$  scattering from the proton target. The momenta of the incoming pion, incoming nucleon and the outgoing nucleon are  $p_1$ ,  $p_2$  and  $p'_2$ , respectively. The pion and the nucleon masses are both neglected,  $p_1^2 = 0$ ,  $p_2^2 = (p'_2)^2 = 0$ . We denote the momenta of the outgoing quark and antiquark (jets) as  $q_1$  and  $q_2$ , respectively. They are on the mass shell,  $q_1^2 = q_2^2 = 0$ . We will use the Sudakov decomposition of 4-vectors with respect to the momenta of the incoming particles  $p_1$  and  $p_2$ . For instance, the jet momenta are decomposed according to

$$q_1 = zp_1 + \frac{q_{1\perp}^2}{zs}p_2 + q_{1\perp}, q_2 = \bar{z}p_1 + \frac{q_{2\perp}^2}{\bar{z}s}p_2 + q_{2\perp} \quad (1.1)$$

such that  $z$  is the longitudinal momentum fraction of the quark jet in the lab frame. We will often use the shorthand notation:  $\bar{u} \equiv (1-u)$  for any longitudinal momentum fraction  $u$ . The Dirac spinors for the quark and the antiquark are denoted by  $\bar{u}(q_1)$  and  $v(q_2)$ .

We are interested in the forward limit, when the transferred momentum  $t = (p_2 - p'_2)^2$  is equal to zero<sup>†</sup>, and the transverse momenta of jets compensate each other  $q_{1\perp} \equiv q_{\perp}$ ,  $q_{2\perp} \equiv -q_{\perp}$ . In this kinematics the invariant mass of the produced  $q\bar{q}$  pair is equal to  $M^2 = q_{\perp}^2/z\bar{z}$ . The invariant c.m. energy  $s = (p_1 + p_2)^2 = 2p_1 p_2$  is taken to be much larger

<sup>†</sup>If the target mass  $m$  is taken into account, the momentum transfer  $t = (p_2 - p'_2)^2$  contains a non-vanishing longitudinal contribution and is constrained from below by  $|t| \geq t_0$ , where  $t_0 = (m^2 M^4)/(s - m^2)^2$ ,  $M^2$  being the invariant mass of the dijet.

than the transverse jet momentum  $q_\perp$ . In what follows we often neglect contributions to the amplitude that are suppressed by powers of  $q_\perp^2/s$ .

From the theoretical point of view, the principal question is whether the relevant transverse size of the pion  $r_\perp$  remains small, of the order of the inverse transverse momenta of the jets  $r_\perp \sim 1/q_\perp$ . In this paper we investigate the possibility that the amplitude of hard dijet coherent production can be calculated using the standard collinear factorization in the form suggested by Fig. 1:

$$\mathcal{M}_{\pi \rightarrow 2 \text{jets}} = \sum_{p=q,\bar{q},g} \int_0^1 dz' \int_0^1 dx_1 \phi_\pi(z', \mu_F^2) T_H^p(z', x_1, \mu_F^2) F_\zeta^p(x_1, \mu_F^2). \quad (1.2)$$

Here  $\phi_\pi(z', \mu_F^2)$  is the pion distribution amplitude, and  $F_\zeta^p(x_1, \mu_F^2)$  is the generalized (skewed) parton distribution  $p = q, \bar{q}, g$  [22, 23, 24] in the target nucleon or nucleus;  $x_1$  and  $x_2 = x_1 - \zeta$  are the momentum fractions of the emitted and the absorbed partons, respectively. The asymmetry parameter  $\zeta$  is fixed by the process kinematics:

$$\zeta = M^2/s = q_\perp^2/z\bar{z}s. \quad (1.3)$$

$T_H(z', x_1, \mu_F^2)$  is the hard scattering amplitude involving at least one hard gluon exchange and  $\mu_F$  is the (collinear) factorization scale. By definition, the pion distribution amplitude only involves small momenta,  $k_\perp < \mu_F$ , and the hard scattering amplitude is calculated neglecting the parton transverse momenta. In this paper we present a detailed calculation of the leading-order contribution to  $T_H(z', x_1, \mu_F^2)$  corresponding to a single hard gluon exchange.

We consider both the quark and the gluon contribution to the amplitude, and in both cases find that the corresponding hard kernels  $T_H^q$ ,  $T_H^g$  diverge as  $1/z'^2$  and  $1/\bar{z}'^2$  in the  $z' \rightarrow 0$  and  $z' \rightarrow 1$  limit, respectively. This implies that the integration of the pion momentum fraction diverges at the end-points and the collinear factorization is, therefore, broken. Physically this means that the approximation of neglecting the incident quark transverse momenta becomes insufficient close to the end points, similar to what happens e.g. in the heavy quark limit in B-decays [25], albeit for a different reason. One may argue that Sudakov-type radiative corrections should suppress the end-point contributions and try to develop a modified factorization framework, by the resummation of soft gluon emission to all orders [26]. Alternatively, the end-point singularities may be softened on a nuclear target because of the color filtering of configurations with a large transverse size. Both possibilities are interesting and require detailed studies that go far beyond the tasks of this paper. We will rather assume that the end-point behavior can be tamed in some reasonable way, and examine the consequences.

In particular, we will analyze the structure of the hard gluon exchange contribution in some detail. We will find that the structure of this exchange is such that it generates an enhancement by a logarithm of the energy in the region  $|z' - z| \ll 1$ . If only this logarithmic contribution is retained, the collinear factorization is restored and the longitudinal momentum distribution of the jets to this accuracy indeed follows the shape of the pion distribution amplitude [13]. The hard gluon exchange can in this case be considered as

a part of the unintegrated gluon distribution, as advocated in [17]. Beyond the leading logarithms in energy this proportionality does not hold. Remarkably enough, we find that the longitudinal momentum fraction distribution of the jets for the non-factorizable contribution is calculable, and turns out to be the same as for the factorizable contribution with the asymptotic pion distribution amplitude. We also find, in agreement with [21] that the quark contribution is significant in the energy range of the E-791 experiment and present a new data analysis including all contributions. On the technical side, we present a detailed study of the light-cone limit of the relevant amplitudes, the structure of different absorption parts and the gauge-dependence. We believe that some of this discussion is of general interest and relevant for all exclusive processes in the diffractive kinematics.

The presentation is organized as follows. In Sec. 2 we consider the quark contribution to the coherent dijet production, which is simpler than the gluon contribution as it does not involve subtleties related to the choice of the gauge. We find an end-point singularity in the integration over the pion quark (antiquark) momentum fraction and trace its origin to pinching of the integration contour over the partonic momentum fraction in the so-called Glauber region. We explain this result by analyzing the structure of different dispersion parts of the amplitude. The gluon contribution is considered in Sec. 3. We point out that there is a subtlety in the definition of the generalized gluon distribution, and explain how this subtlety is resolved in a more familiar case of hard electroproduction of vector mesons. Next, we present a calculation of the imaginary part of the amplitude of the coherent dijet production from a quark, in which the above-mentioned problem is avoided. Finally, we perform the calculation of the full amplitude (including the real part) using axial gauge and not assuming the light-cone dominance from the beginning. Similar as in the quark case, we observe pinching of singularities between soft gluon interactions in the initial and the final states. A detailed numerical analysis and the comparison to the E791 data is presented in Sec. 4, while Sec. 5 is reserved for the conclusions.

One technical remark is in order. Calculations in the main text are presented using Radyushkin's definitions [6, 23] for the generalized parton distributions. The relation to the more commonly used symmetric notation by Ji [24] is explained in App. A and in App. B we collect all the final expressions in the symmetric notation.

## 2 The Quark Contribution

### 2.1 The Calculation

We begin with the calculation of the quark contribution to the hard dijet production, which is simpler than the gluon contribution as it does not involve subtleties related to the choice of the gauge. For definiteness we consider  $\pi^-$ -proton scattering. The quark contribution starts at order  $\mathcal{O}(\alpha_s^2)$  and can be decomposed in three topologically different contributions shown in Fig. 2, Fig. 3 and Fig. 4. In what follows we refer to them as the  $u$ -quark annihilation, the  $d$ -quark exchange, and the gluon exchange (flavor-singlet) contribution, respectively. All three contributions are separately gauge invariant and can be calculated with quarks on the mass shell. In this section we work in the Feynman gauge.

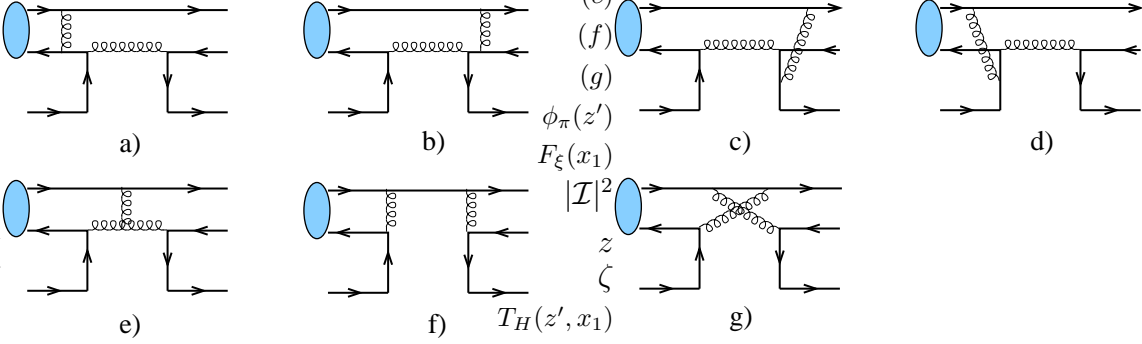


Figure 2: The  $u$ -quark (annihilation) contribution to the coherent hard dijet production  $\pi^- \rightarrow 2$  jets, see text.

The antiquark contributions do not require a new calculation and can be obtained from the corresponding quark contributions by obvious substitutions, see below. The reaction kinematics and the notation for the momenta are specified in the Introduction. We define the generalized quark (antiquark) distribution as the matrix element of the light-cone operator [6, 23]

$$\langle p'_2 | \bar{q}(0) \not{y} q(y) | p_2 \rangle_{y^2=0} = \bar{u}(p'_2) \not{y} u(p_2) \cdot \int_0^1 dx_1 [e^{-ix_1(p_2 y)} \mathcal{F}_\zeta^q(x_1) - e^{ix_2(p_2 y)} \mathcal{F}_\zeta^{\bar{q}}(x_1)], \quad (2.1)$$

where  $q = u, d, \dots$ , etc. Hereafter we use the notation

$$x_2 = x_1 - \zeta, \quad (2.2)$$

where the asymmetry parameter  $\zeta$  is defined as  $p_2 - p'_2 = \zeta p_2$  and is fixed by the kinematics of the reaction, see (1.3). The relation to other common parametrizations of the generalized parton distributions is discussed in Appendix A. In turn, the pion distribution amplitude is defined as [1, 2, 3]

$$\langle 0 | \bar{d}(0) \not{y} \gamma_5 u(y) | \pi^-(p_1) \rangle_{y^2=0} = i(p_1 y) f_\pi \int_0^1 dz' e^{-iz'(p_1 y)} \phi_\pi(z'), \quad \int_0^1 dz' \phi_\pi(z') = 1, \quad (2.3)$$

where  $f_\pi = 133$  MeV is the pion decay constant. In both cases, (2.1) and (2.3), the insertion of the path-ordered gauge factor between the quark field operators is implied. Both distributions depend on the factorization scale  $\mu_F$  which to the leading logarithmic accuracy has to be taken of the order of the transverse momentum of the jets.

As an example, consider the first diagram in Fig. 2. The corresponding contribution reads:

$$\begin{aligned} i\mathcal{M}_{2a} = & -(ig)^4 (-i)^2 (i) \int_0^1 dz' \frac{if_\pi \phi_\pi(z')}{4N_c} \int_0^1 dx_1 \frac{\mathcal{F}_\zeta^u(x_1) \sqrt{1-\zeta}}{2N_c} (t^a t^a t^b t^b)_{ij} \\ & \times \frac{\bar{u}(q_1) \gamma_\mu \gamma_5 \not{p}_1 \gamma_\mu (\zeta \not{p}_2 - \not{q}_2) \gamma_\nu \not{p}_2 \gamma_\nu v(q_2)}{[(\zeta p_2 - q_2)^2 + i\epsilon][(q_1 - z' p_1)^2][(q_2 + x_2 p_2)^2]}, \end{aligned} \quad (2.4)$$

where  $\bar{u}(q_1)$  and  $v(q_2)$  are Dirac spinors for the outgoing quark and antiquark jets, respectively, and  $i, j$  are the jet color indices. The color state of the target quark is averaged over. Note that we only show the Feynman  $+i\epsilon$  prescription for one of the propagators, since the other two are strongly off-shell.

A simple calculation yields

$$\mathcal{M}_{2a} = \frac{4\pi^2\alpha_s^2 if_\pi}{N_c^2 q_\perp^2} \sqrt{1-\zeta} \bar{u}(q_1) \gamma_5 \frac{p_2}{s} v(q_2) \delta_{ij} \int_0^1 dz' \phi_\pi(z') \int_0^1 dx_1 \mathcal{F}_\zeta^u(x_1) \cdot I_{2a}(z, z', x_1, x_2) \quad (2.5)$$

with the coefficient function

$$I_{2a}(z, z', x_1, x_2) = -\frac{2C_F^2 z}{z' \bar{z}(x_2 + i\epsilon)}, \quad (2.6)$$

where  $C_F = (N_c^2 - 1)/(2N_c)$ ,  $N_c$  is the number of colors. Calculation of the other diagrams in Fig. 2 is equally simple. The corresponding coefficient functions are

$$\begin{aligned} I_{2b}(z, z', x_1, x_2) &= \frac{2C_F^2 z}{z' \bar{z}'[x_1 + i\epsilon]}, \\ I_{2c}(z, z', x_1, x_2) &= -\frac{C_F z(\zeta z - x_1)}{N_c z' \bar{z}'[x_1 + i\epsilon][x_1(z - z') - z \bar{z}' \zeta + i\epsilon]}, \\ I_{2d}(z, z', x_1, x_2) &= -\frac{C_F z(\zeta z' - x_1)}{N_c z' \bar{z}[x_2 + i\epsilon][x_1(z' - z) - z' \bar{z} \zeta + i\epsilon]}, \\ I_{2e}(z, z', x_1, x_2) &= \frac{C_F N_c z(x_1 + \zeta(1 - z - z'))}{z' \bar{z}' \bar{z}[x_1 + i\epsilon][x_2 + i\epsilon]}, \\ I_{2f}(z, z', x_1, x_2) &= -\frac{2C_F^2 \zeta z}{\bar{z}'[x_1 + i\epsilon][x_2 + i\epsilon]}, \\ I_{2g}(z, z', x_1, x_2) &= -\frac{C_F \zeta^2 z(1 - z - z')}{N_c \bar{z}'[x_1 + i\epsilon][x_2 + i\epsilon][x_1(1 - z - z') - \bar{z} \bar{z}' \zeta + i\epsilon]}, \end{aligned} \quad (2.7)$$

so that the total contribution of the  $u$ -quark annihilation is given by the expression in (2.5) with the coefficient function

$$I(z, z', x_1, x_2) = \sum_{i=2a,2b,\dots,2g} I_i(z, z', x_1, x_2) \quad (2.8)$$

instead of  $I_{2a}$ .

The  $d$ -quark exchange contributions in Fig. 3 can be obtained from the corresponding diagrams in Fig. 2 by the substitution:  $x_1 \rightarrow -x_2$ ,  $x_2 \rightarrow -x_1$ ,  $z \rightarrow \bar{z}$ ,  $z' \rightarrow \bar{z}'$  and an overall minus sign. Similarly, the antiquark  $\bar{d}$ -annihilation and  $\bar{u}$ -exchange coefficient functions can be obtained from the above expressions by the substitution  $x_1 \rightarrow -x_2$ ,  $x_2 \rightarrow -x_1$  and changing the overall sign. Altogether, we obtain four coefficient functions:

$$I_u(z, z', x_1, x_2) = I(z, z', x_1, x_2),$$

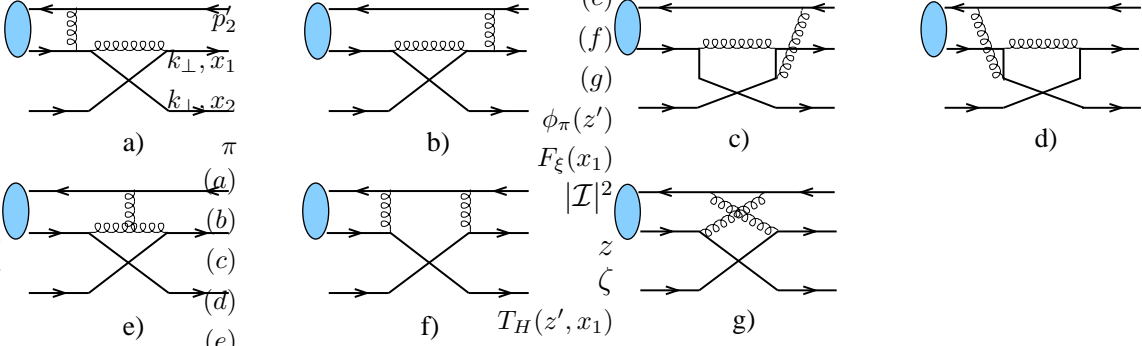


Figure 3: The  $d$ -quark (exchange) contribution to the coherent hard dijet production  $\pi^- \rightarrow 2$  jets, see text. Note that the quark and the antiquark lines entering the pion blob are interchanged compared to Fig. 2.

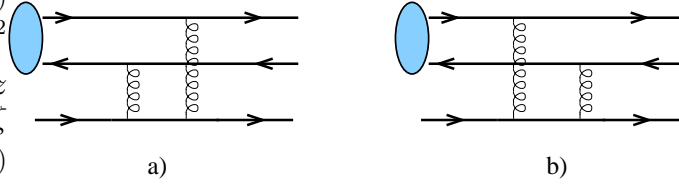


Figure 4: The flavor-singlet quark contribution to the coherent hard dijet production  $\pi \rightarrow 2$  jets.

$$\begin{aligned}
 I_d(z, z', x_1, x_2) &= -I(\bar{z}, \bar{z}', -x_2, -x_1), \\
 I_{\bar{u}}(z, z', x_1, x_2) &= -I(z, z', -x_2, -x_1), \\
 I_{\bar{d}}(z, z', x_1, x_2) &= I(\bar{z}, \bar{z}', x_1, x_2).
 \end{aligned} \tag{2.9}$$

Last but not least, we have to take into account the diagrams in Fig. 4 corresponding to the flavor-singlet two-gluon exchange. Note that the virtuality of both gluons is large, in fact equal to the transverse momentum of the jets, and, therefore, these diagrams are part of the quark coefficient function rather than the gluon one. A simple calculation yields

$$\begin{aligned}
 I_{4a}(z, z', x_1, x_2) &= -\frac{C_F(\zeta(1+z-z')-2x_1)}{z'z'\zeta[x_1(z-z')-z\bar{z}'\zeta+i\epsilon]}, \\
 I_{4b}(z, z', x_1, x_2) &= -\frac{C_F(\zeta(1-z+z')-2x_1)}{z'z'\zeta[x_1(z'-z)-z'\bar{z}\zeta+i\epsilon]}.
 \end{aligned} \tag{2.10}$$

Denoting the sum of them as

$$I_{\text{glue}} = I_{4a} + I_{4b} \tag{2.11}$$

we obtain the final answer for the leading-order quark contribution to the dijet production in the form

$$\begin{aligned}
 \mathcal{M}_{\text{quark}} &= \frac{4\pi^2\alpha_s^2 if_\pi}{N_c^2 q_\perp^2} \sqrt{1-\zeta} \bar{u}(q_1) \gamma_5 \frac{\not{p}_2}{s} v(q_2) \delta_{ij} \int_0^1 dz' \phi_\pi(z') \int_0^1 dx_1 \\
 &\quad \times \sum_p \mathcal{F}_\zeta^p(x_1) \left[ I_{\text{glue}}(z, z', x_1, x_2) + I_p(z, z', x_1, x_2) \right],
 \end{aligned} \tag{2.12}$$

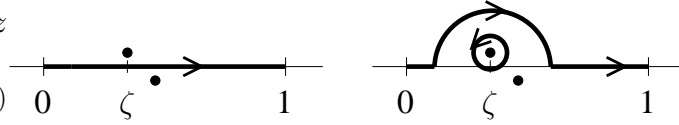


Figure 5: Deformation of the integration contour in the complex  $x_1$  plane in the Glauber region, see text.

where the summation goes over all possible quark-parton species:  $p = u, \bar{u}, d, \bar{d}$ , etc.

## 2.2 The End-Point Behavior

Next, we have to examine the behavior of the coefficient functions  $I_{glue}$  and  $I_p$  at the end points  $z' \rightarrow 0$  and  $z' \rightarrow 1$  and check the convergence of the integration in (2.12) over the quark momentum fraction  $z'$  in the pion. Convergence is necessary for the self consistency of the collinear factorization approach as it ensures that quark transverse momenta in the pion can be neglected.

Consider the gluon-exchange contribution  $I_{glue}$  first. In this case it is easy to see that  $I_{glue} \sim 1/z'$  and  $I_{glue} \sim 1/\bar{z}'$  at  $z' \rightarrow 0$  and  $z' \rightarrow 1$ , respectively. Since the pion distribution amplitude vanishes linearly at the end-points, at least at a sufficiently high scale, the corresponding contribution to the result in (2.12) is finite.

From Eqs. (2.6) and (2.7) it is seen that the contributions of the  $u$ -quark and  $\bar{d}$ -antiquark are finite as well<sup>‡</sup>. For the  $d$ -quark and the  $\bar{u}$ -antiquark contributions the situation is different, however. In this case we find

$$I^d(z, z', x_1, x_2)|_{z' \rightarrow 0} = \frac{2i\pi C_F}{N_c} \frac{\bar{z}}{z z'^2} \delta(x_2) + \mathcal{O}\left(\frac{1}{z'}\right), \quad (2.13)$$

and

$$I^{\bar{u}}(z, z', x_1, x_2)|_{z' \rightarrow 1} = \frac{2i\pi C_F}{N_c} \frac{z}{\bar{z} \bar{z}'^2} \delta(x_2) + \mathcal{O}\left(\frac{1}{\bar{z}'}\right). \quad (2.14)$$

Note that: a) the  $\sim 1/z'^2$  ( $\sim 1/(\bar{z}')^2$ ) behavior leads to the logarithmically divergent integral over the pion quark momentum fraction; b) this contribution is purely imaginary, and c) this contribution is proportional to  $\delta(x_2) = \delta(x_1 - \zeta)$ , i.e. it is due to parton configurations with vanishing longitudinal momentum fraction of one of the quarks in the target proton. In the terminology of [27] this corresponds to the Glauber region. In the remaining part of this Section we explain this result for the example of the  $d$ -quark contribution in some detail.

Explicit expressions for the diagrams in Fig. 3 can be obtained from Eqs. (2.6), (2.7) using the substitution rules in (2.9). One can easily convince oneself that the only diagrams capable of producing a  $\sim 1/z'^2$  singularity are those in Fig. 3c and Fig. 3g. In particular, the diagram in Fig. 3c gives:

$$I_{3c}(z, z', x_1, x_2) = -\frac{C_F \bar{z}(\bar{z} + x_2)}{N_c z' \bar{z}' [x_2 - i\epsilon] [x_2(z - z') - z' \bar{z} \zeta + i\epsilon]}. \quad (2.15)$$

<sup>‡</sup>We remind that the flavor identification refers to the particular case of  $\pi^-$  meson scattering.

It is seen that for finite values of  $x_2$  this contribution is proportional to  $1/z'$  to the first power. However, as  $z' \rightarrow 0$  the two poles in the Feynman denominators in Eq. (2.15) produce a pinch at  $x_2 = 0$  ( $x_1 = \zeta$ ) in the integral over  $x_1$ , see Fig. 5. This pinch is responsible for the singular behavior of  $I_{3c}$ ,  $I_{3c} \sim 1/z'^2$ . To see this, note that if the two poles would lie on the same side of the integration contour, the singularity at  $x_2 = 0$  could be avoided by the contour deformation, following the arguments of Ref. [28] (see also [7]). In the presence of the pinch one can also deform the contour, but in this case an additional contribution arises

$$I_{3c}^{\text{pole}}(z, z', x_1, x_2) = \frac{2i\pi C_F}{N_c} \frac{\bar{z}}{z'^2} \delta(x_2) . \quad (2.16)$$

This pole contribution is entirely responsible for the leading asymptotics of  $I_{3c}$  in the  $z' \rightarrow 0$  region. The calculation of the diagram in Fig. 3g is very similar. In this case also one can deform the contour as it is shown at Fig. 5 and the leading asymptotics of  $I_{3g}$  is again given by the pole contribution

$$I_{3g}^{\text{pole}}(z, z', x_1, x_2) = \frac{2i\pi C_F}{N_c} \frac{\bar{z}^2}{zz'^2} \delta(x_2) . \quad (2.17)$$

The sum of these pole contributions gives the result in (2.13). For the  $\bar{u}$ -contribution, again, the pinch at  $x_1 = \zeta$  appears at  $z' \rightarrow 1$  and leads to the result (2.14).

The pinching of integration contours in the Glauber region indicates a serious problem with collinear factorization. It is known [29] that such pinches generally occur between initial and final state interactions involving soft particle (gluon) exchanges. In the case of the Drell-Yan production the pinches disappear in the sum of all Feynman diagrams for the cross section, which is due, in physical terms, to cancelation of the final state interactions [28] (see also [30]). In our case the pinch occurs in the leading-order contribution and for quark exchange, which is unusual. Note that the problem with pinching singularities in the Glauber region is in principle unrelated to the end-point behavior of the pion distribution amplitude and is more general. We will return to this discussion in the next section.

Our result in (2.12) differs from the expression for the quark contribution obtained in [21] by the above discussed pole terms. The authors of [21] have restored the imaginary part of the coefficient function by requiring that the physical amplitude only depends on  $s + i\epsilon$  and hence on  $\zeta - i\epsilon$  (with the real integration variable  $x_1$ ). It is easy to see that with this prescription all singularities in the denominators are below the integration contour and do not obstruct the analytic continuation. In this sense, this prescription corresponds to the “true” light-cone contribution. The argument is not correct, however, since apart from the usual  $s$ -channel discontinuity the amplitude in question has a discontinuity in another invariant variable,  $M^2$ , the invariant mass of the jets. The full imaginary part is only restored in their sum and the existence of two different types of cuts is reflected in the structure of Feynman  $i\epsilon$  prescription in the propagators. To explain this point, consider the different dispersion parts corresponding to the diagrams in Fig. 2c and Fig. 3c, see Fig. 6.

It is obvious that the cut diagrams denoted as 2c-I and 2c-III describe the discontinuity in the invariant energy  $s$ , and the cut diagram 2c-II corresponds to the discontinuity in the  $M^2$ -variable. Note that in the light-cone limit the  $s$ -channel cut 2c-I and the  $M^2$ -channel

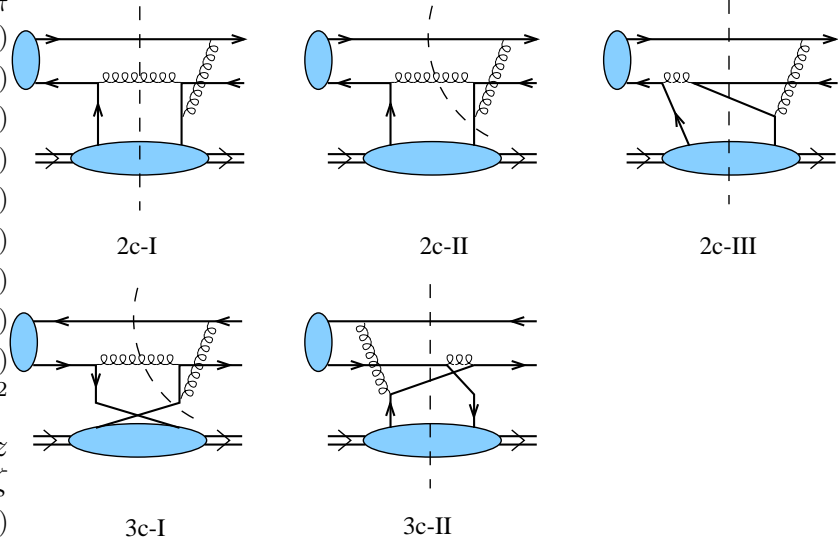


Figure 6: Different dispersion parts corresponding to the diagrams in Fig. 2c and Fig. 3c.

cut 2c-II both occur at  $x_1 = 0$ , see (2.7). Moreover, their contributions exactly cancel each other. In the usual language this cancellation manifests itself in the following way. The part of the coefficient function,  $I_{2c}(z, z', x_1, x_2)$ , which corresponds to the diagram in Fig. 2c has a pole at  $x_1 \rightarrow 0$ . This pole does not contribute, however, to the imaginary part of the amplitude since the generalized quark distribution function vanishes at this point,  $\mathcal{F}_\zeta(x)|_{x \rightarrow 0} \rightarrow 0$  [23, 7]. As the result, we are left with the single s-channel cut 2c-III corresponding to the  $[x_1(z - z') - z\bar{z}'\zeta + i\epsilon]$  denominator in  $I_{2c}(z, z', x_1, x_2)$ . Note that the Feynman  $i\epsilon$  prescription to go around the pole is in agreement with the above statement that it corresponds to a singularity in the s-channel: The sign of  $i\epsilon$  can be understood as the substitution  $s \rightarrow s + i\epsilon$ , or  $\zeta \rightarrow \zeta - i\epsilon$ .

Now let us turn over to the dispersion parts of the diagram corresponding to Fig. 3c. In this case there are two possible cuts 3c-I and 3c-II that describe the singularities in the  $M^2$ - and s-channels, respectively. The corresponding coefficient function  $I_{3c}(z, z', x_1, x_2)$  contain two poles, see eq. (2.15). The  $[x_2 - i\epsilon] = [x_1 - \zeta - i\epsilon]$  pole is related to the  $M^2$ -channel discontinuity and its  $i\epsilon$  prescription corresponds to the substitution  $M^2 \rightarrow M^2 + i\epsilon$ , or  $\zeta \rightarrow \zeta + i\epsilon$ . On the other hand, the  $i\epsilon$  prescription of the second denominator  $[x_2(z - z' - z')\bar{z} + i\epsilon]$  can be understood as the substitution  $s \rightarrow s + i\epsilon$ , or  $\zeta \rightarrow \zeta - i\epsilon$ , in agreement with the interpretation that this singularity occurs in the s-channel. To summarize, we see that for the case of the diagram in Fig. 3c both dispersion parts contribute in a nontrivial way and pinching of the integration contour described above in fact occurs between the discontinuities in different channels. It is also seen that the pinching occurs between the soft quark exchange in the initial state (3c-I) and in the final state (3c-II) with respect to the hard interaction, in agreement with the general arguments in [29].

### 3 Gluon Contribution

The gluon contribution to hard dijet production is more involved because of subtleties related to gauge invariance. One is tempted to calculate the coefficient function in front of the gluon distribution by considering pion scattering from on-shell gluons with zero transverse momentum, similar to the above calculation for the quarks. The result has in this case to be multiplied by the gluon distribution in the target in the physical light-cone gauge  $p_1^\mu A_\mu = 0$ , which has the form [4, 23]

$$\langle p'_2 | A_\mu^a(0) A_\nu^a(y) | p_2 \rangle_{y^2=0} = -\frac{\bar{u}(p'_2) \not{p}_1 u(p_2)}{2(p_1 p_2)} g_{\mu\nu}^\perp \int_0^1 dx_1 \frac{1}{2} [e^{-ix_1(p_2 y)} + e^{ix_2(p_2 y)}] \frac{\mathcal{F}_\zeta^g(x_1)}{x_1 x_2}, \quad (3.1)$$

where

$$g_{\mu\nu}^\perp = g_{\mu\nu} - \frac{p_{1\mu} p_{2\nu} + p_{1\nu} p_{2\mu}}{(p_1 p_2)}. \quad (3.2)$$

The difficulty arises because of the factor  $1/(x_1 x_2)$  which is singular within the integration domain. The particular procedure to deal with this singularity is related to the gauge condition for the gluon field at time infinity and has to be established by considering carefully the light-cone limit of the relevant Feynman diagrams. For the classical process of hard vector meson production by longitudinally polarized photons [8, 4] the correct prescription was formulated by Radyushkin [23]

$$\frac{1}{x_1 x_2} \rightarrow \frac{1}{(x_1 - i\epsilon)(x_2 + i\epsilon)}. \quad (3.3)$$

It is not obvious, however, whether the same substitution is true for the hard dijet production. In fact, we will argue that no simple prescription exists in this case at all. In order to find the answer, in this section we will not assume zero gluon transverse momentum from the beginning, but consider instead the full scattering amplitude of the hard dijet production from the quark target mediated by the two-gluon exchange, cf. Fig. 1. We will identify the (IR divergent) contribution to this amplitude corresponding to the region of small gluon transverse momenta and try to find a factorized expression for it, as a product of the coefficient function times the perturbative gluon distribution in a quark.

For pedagogical reasons, we first consider the simpler case of hard vector meson production by longitudinally polarized photons. We do the calculation in Feynman and in the light-cone gauge and explain how the prescription in (3.3) arises in both cases. Next, we present the calculation of the imaginary part of the amplitude for hard dijet production in Feynman gauge. This calculation was previously reported by us in [19]. Finally, we derive the full expression for the amplitude (both real and imaginary part) using the axial gauge and compare our results to the work [20].

#### 3.1 Getting Started: Exclusive Vector Meson Production

To the lowest order in  $\alpha_s$  the relevant Feynman diagrams are shown in Fig. 7. The kinematics is similar to that of the dijet production. We take  $p_2$  and  $p'_2$  to be the target

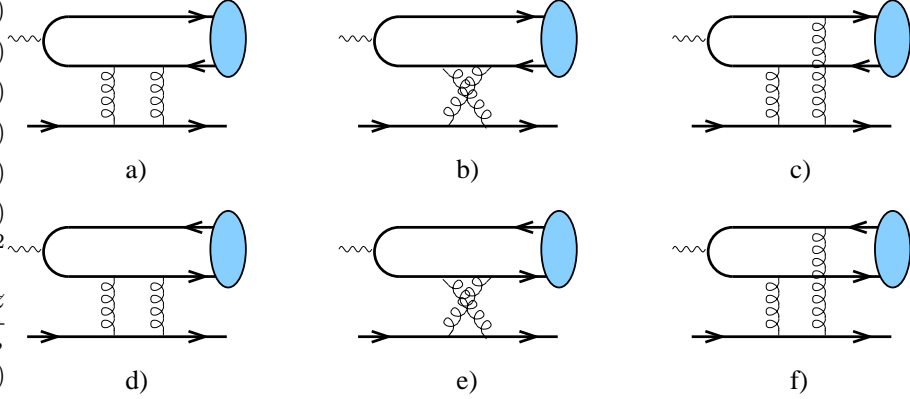


Figure 7: The leading-order gluon contribution to the hard exclusive vector meson production  $\gamma^* \rightarrow \rho^0$ .

quark momenta in the initial and the final state, respectively. The momentum of the vector meson in the final state is denoted by  $p_1$ . The virtual photon momentum is equal to  $q = p_1 - \zeta p_2$  and we use the further notations  $Q^2 = -q^2$  and  $\zeta = Q^2/s$  with  $s = 2p_1 p_2$ . We take the photon to be longitudinally polarized, with the polarization vector

$$e_\mu^L = \frac{1}{Q} p_{1,\mu} + \frac{Q}{s} p_{2,\mu} = \frac{1}{Q} q_\mu + 2 \frac{Q}{s} p_{2,\mu}, \quad e_\mu^L q^\mu = 0, \quad e_L^2 = 1. \quad (3.4)$$

Thanks to the  $U(1)$  gauge invariance one can omit the first term in the above expression and use a simpler vector

$$e_\mu^L \rightarrow e_\mu^L = 2 \frac{Q}{s} p_{2,\mu}. \quad (3.5)$$

The vector meson distribution amplitude is defined by the expression similar to (2.3)

$$\langle 0 | \bar{q}(0) \not{y} q(y) | V(p_1) \rangle_{y^2=0} = f_V(p_1 y) \int_0^1 dz e^{-iz(p_1 y)} \phi_V(z), \quad (3.6)$$

where  $f_V$  is the corresponding decay constant. For simplicity we do not elaborate on the isospin structure and consider below the contribution of the single light quark flavor  $q$ . The variable  $z$  corresponds to the momentum fraction carried by the quark. In the calculation of the amplitude sandwiched between the two target quark spinors  $\bar{u}(p'_2)$  and  $u(p_2)$  we will assume averaging over the color of the target quark and make the replacement

$$\bar{u}(p'_2) \mathcal{M} u(p_2) \rightarrow \frac{\sqrt{1-\zeta}}{2} \text{Sp}[\mathcal{M} \not{p}_2] \quad (3.7)$$

picking up contribution of the unpolarized gluon distribution, which is dominant at large energies.

For definiteness, consider the contribution of the diagram in Fig. 7a. We obtain

$$\begin{aligned} i\mathcal{M}_a &= \sqrt{4\pi\alpha} e_q g^4 f_V \sqrt{1-\zeta} \frac{1}{8N_c} C_F \int \frac{d^4 k}{(2\pi)^4} \int_0^1 dz \phi_V(z) \\ &\times \text{Tr} \left[ \not{p}_1 \left( \frac{2Q}{s} \right) \not{p}_2 \frac{(z \not{p}_1 - \not{q})}{(zp_1 - q)^2 + i\epsilon} \gamma_{\mu_1} \frac{(\zeta \not{p}_2 - \not{k} - \bar{z} \not{p}_1)}{(\zeta p_2 - k - \bar{z} p_1)^2 + i\epsilon} \gamma_{\mu_2} \right] \mathcal{R}_{\mu_1 \mu_2}, \end{aligned} \quad (3.8)$$

where  $e_q$  is the quark electric charge,  $\alpha = 1/137$  is the fine structure constant, and

$$\mathcal{R}_{\mu_1\mu_2} = \frac{1}{2} \text{Tr} \left[ \not{p}_2 \gamma_{\nu_2} \frac{(\not{p}_2 - \not{k})}{(p_2 - k)^2 + i\epsilon} \gamma_{\nu_1} \right] \frac{N_{\mu_1\nu_1}(k) N_{\mu_2\nu_2}(k - \zeta p_2)}{[k^2 + i\epsilon][(k - \zeta p_2)^2 + i\epsilon]} \quad (3.9)$$

is a common factor for all Feynman diagrams in Fig. 7 that describes the emission of the pair of gluons from the target quark line. In the expression for  $\mathcal{R}$  we have assumed a general form for the gluon propagator

$$D_{\mu\nu}(k) = \frac{-i}{k^2 + i\epsilon} N_{\mu\nu}. \quad (3.10)$$

In order to do the integration over the loop momentum we use the Sudakov parametrization

$$k = \alpha p_1 + x_1 p_2 + k_\perp, \quad d^4 k = \frac{s}{2} d\alpha dx_1 d^2 k_\perp, \quad k^2 = \alpha x_1 s - k_\perp^2 \quad (3.11)$$

and take the integral over  $\alpha$  by residues. After this, the integration over  $x_1$  gets confined to the interval  $0 \leq x_1 \leq 1$  and the variable  $x_1$  acquires the meaning of the longitudinal momentum fraction. In the Feynman gauge  $N_{\mu\nu} = g_{\mu\nu}$  we obtain after some algebra

$$\mathcal{M}_a = \sqrt{4\pi\alpha} e_q f_V \sqrt{1-\zeta} \frac{Q}{s} \frac{C_F g^4}{16\pi^3 N_c} \int_0^1 dz \phi_V(z) \int d^2 k_\perp \int_0^1 dx_1 I_a \quad (3.12)$$

with

$$I_a = \frac{1}{k_\perp^4 \bar{z} \zeta (1-\zeta)} \left[ \frac{\bar{z} s (2s(1-x_1)^2 \bar{z} + k_\perp^2 x_2)}{[s\bar{z}x_2 - k_\perp^2(1-\zeta)/(1-x_1) + i\epsilon]} \right. \\ \left. + \Theta(-x_2) \frac{2s(1-x_1)\bar{z}x_2 + k_\perp^2(2-x_1-\zeta)}{x_2 \zeta} \right]. \quad (3.13)$$

The contribution of large transverse momenta  $k_\perp \geq Q$  in Eq. (3.12) gives rise to the  $\alpha_s^2$  correction to the coefficient function in front of the quark distribution in the target and is not relevant for our discussion. We concentrate, therefore, on the region of small  $k_\perp \ll Q$ . Notice that the  $k_\perp$  integral is infrared (IR) divergent. The quadratic divergence  $dk_\perp^2/k_\perp^4$  must cancel in the sum of all Feynman diagrams and the remaining logarithmically divergent integral  $\sim dk_\perp^2/k_\perp^2$  has to be interpreted as the perturbative gluon distribution in a quark. In order to observe factorization one has, therefore, to expand the integrand in powers of  $k_\perp^2$  and keep two first terms. The expansion of the denominator in the first term in Eq. (3.13) in the vicinity of  $x_2 = 0$  ( $x_1 = \zeta$ ) may seem dangerous. However, the integral over  $x_1$  can be deformed to the complex plane away from this singularity, and the expansion can be done without further problems. We obtain

$$I_a \stackrel{k_\perp^2 \rightarrow 0}{=} \frac{1}{k_\perp^4 \bar{z} \zeta (1-\zeta)} \left[ \frac{2s(1-x_1)^2 \bar{z} x_2 + k_\perp^2 ((1-x_1)^2 + (1-\zeta)^2)}{(x_2 + i\epsilon)^2} \right. \\ \left. + \Theta(-x_2) \frac{2s(1-x_1)\bar{z}x_2 + k_\perp^2(2-x_1-\zeta)}{x_2 \zeta} \right] + \mathcal{O}(k_\perp^0). \quad (3.14)$$

Since the integration is restricted to the region  $k_\perp^2 \ll Q^2$  the constant terms  $\mathcal{O}(k_\perp^0)$  can be omitted. Note the  $+i\epsilon$  prescription to go around the singularity as a “memory” of the direction in which the analytical continuation to the complex  $x_1$  plane is performed, which, in turn, has its origin in the Feynman  $+i\epsilon$  prescription in the quark propagator  $1/[(\zeta p_2 - k - \bar{z}p_1)^2 + i\epsilon]$ .

Calculation of the other diagrams in Fig. 7 is similar. Here we cite only the final result, cf. [8, 23]:

$$\mathcal{M} = \frac{4\pi\sqrt{4\pi\alpha} e_q \alpha_s f_V}{N_c Q} \int_0^1 dz \frac{\phi_V(z)}{z\bar{z}} \int_0^1 dx_1 \frac{\sqrt{1-\zeta} \mathcal{F}_\zeta^g(x_1)}{(x_1 - i\epsilon)(x_2 + i\epsilon)}, \quad (3.15)$$

where

$$\mathcal{F}_\zeta^g(x) = \frac{\alpha_S}{2\pi} C_F \left[ \frac{1 + (1-x)^2 - \zeta}{1 - \zeta} - \Theta(\zeta - x) \frac{(\zeta - x)(2 - x - \zeta)}{\zeta(1 - \zeta)} \right] \int \frac{dk_\perp^2}{k_\perp^2} \quad (3.16)$$

can be identified with the (perturbative) generalized gluon distribution of a quark<sup>§</sup>. Owing to the  $+i\epsilon$  prescription to go around the singularity at  $x_2 = 0$  the amplitude acquires an imaginary part

$$\text{Im } \mathcal{M} = \frac{-4\pi^2 \sqrt{4\pi\alpha} e_q \alpha_s f_V s}{N_c Q^3} \int_0^1 dz \frac{\phi_V(z)}{z\bar{z}} \mathcal{F}_\zeta^g(\zeta) \sqrt{1 - \zeta}. \quad (3.17)$$

Note that the  $1/k_\perp^4$  terms and the double pole,  $\sim 1/(x_2 + i\epsilon)^2$  present in Eq. (3.14) cancel in the gauge invariant sum of Feynman diagrams, as expected.

For comparison, let us do the same calculation in the light-cone gauge, with the propagator

$$D_{\mu\nu}(k) = \frac{-i}{k^2 + i\epsilon} \left[ g_{\mu\nu} - \frac{k_\mu p_{1\nu} + k_\nu p_{1\mu}}{(kp_1)} \right]. \quad (3.18)$$

For the moment we do not specify a particular prescription to go around the singularity at  $kp_1 = 0$ , this choice will be discussed in detail in what follows.

Using this expression we obtain the following result for the radiation factor (3.9) in the light-cone gauge:

$$\mathcal{R}_{\mu\nu}^{\text{LC}} = \frac{2}{x_1 x_2} \frac{\mathcal{N}_{\mu\nu}}{[k^2 + i\epsilon][(k - \zeta p_2)^2 + i\epsilon][(p_2 - k)^2 + i\epsilon]}, \quad (3.19)$$

where the numerator  $\mathcal{N}_{\mu\nu}$  is equal to

$$\begin{aligned} \mathcal{N}_{\mu\nu} = & (2 - \zeta) k_\mu^\perp k_\nu^\perp + \frac{1}{2} \alpha s x_1 x_2 g_{\mu\nu}^\perp + p_{1\mu} p_{1\nu} [6\alpha k_\perp^2/s + 8\alpha^2(1 - x_1)] \\ & + k_\mu^\perp p_{1\nu} [2k_\perp^2/s + \alpha(4 - 3x_1)] + k_\nu^\perp p_{1\mu} [2k_\perp^2/s + \alpha(4 - 3x_1 - \zeta)] \end{aligned} \quad (3.20)$$

and the prefactor  $1/(x_1 x_2)$  comes from  $1/(kp_1) \cdot 1/[(k - \zeta p_2)p_1]$  in the propagators (3.18) of the  $t$ -channel gluons.

---

<sup>§</sup>Eq. (3.15) is written assuming a single light quark flavor. For  $\rho^0$  meson one has to substitute  $e_q f_V \rightarrow f_\rho/\sqrt{2}$  with  $f_\rho \simeq 200$  MeV.

The integration over the Sudakov variable  $\alpha$  (3.11) converges at values  $\alpha \sim k_\perp^2/s$ . The numerator in (3.19) is, therefore, of order  $\mathcal{O}(k_\perp^2)$  and the radiation factor (3.9) in the light-cone gauge has at most a  $1/k_\perp^2$  singularity at small transverse momenta, compared to  $1/k_\perp^4$  in the Feynman gauge. Because of this, the QCD factorization in light-like gauge is valid for each diagram in Fig. 7 separately: In the upper parts of the diagrams one can substitute  $k = x_1 p_2 + \alpha p_1 + k_\perp \rightarrow x_1 p_2$  and neglect the gluon virtuality and transverse momentum altogether. This is how the parton picture emerges: The amplitude for hard exclusive meson production is given by the convolution of the scattering amplitude off the on-shell transverse gluon  $\gamma^* g \rightarrow V g$  and the gluon distribution in the target quark. In perturbation theory the gluon distribution is given by the integral

$$\int d\alpha \int d^2 k_\perp \mathcal{R}_{\mu\nu}^{\text{LC}} \sim g_{\mu\nu}^\perp \frac{\mathcal{F}_\zeta^g(x_1)}{x_1 x_2}. \quad (3.21)$$

In fact, only the two first terms in (3.20) contribute. Performing the integral over  $\alpha$  and averaging over the directions of  $k_\perp$  we indeed reproduce the result in Eq. (3.16).

The argument presented above is standard and tacitly assumes that the singularities at  $x_2 \rightarrow 0$  and  $x_1 \rightarrow 0$  play no rôle<sup>¶</sup>. In order to recover the correct prescription in Eq. (3.15) we have to be more careful. By the explicit calculation of the six diagrams in Fig. 7 we obtain the following expression:

$$\mathcal{M} = \frac{i\alpha_s}{4\pi^3} \int \frac{d(\alpha s) dx_1 d^2 k_\perp [(2-\zeta)k_\perp^2 - (\alpha s)x_1 x_2] \sqrt{1-\zeta}}{x_1 x_2 [(\alpha s)x_1 - k_\perp^2 + i\epsilon][(\alpha s)x_2 - k_\perp^2 + i\epsilon][(\alpha s)(x_1 - 1) - k_\perp^2 + i\epsilon]} \cdot J \quad (3.22)$$

where

$$J = \frac{2\pi\sqrt{4\pi\alpha} e_q \alpha_s f_V}{N_c Q} \int_0^1 dz \phi_V(z) \left[ \frac{x_2 s}{[(\alpha + \bar{z})s x_2 - k_\perp^2 + i\epsilon]} - \frac{x_1 s}{[(\alpha - z)s x_1 - k_\perp^2 + i\epsilon]} \right. \\ \left. - \frac{k_\perp^2(\zeta s)}{[(\alpha + \bar{z})s x_2 - k_\perp^2 + i\epsilon][(\alpha - z)s x_1 - k_\perp^2 + i\epsilon]} + (z \leftrightarrow \bar{z}) \right]. \quad (3.23)$$

The three terms in the square brackets in (3.23) correspond to the diagrams in Fig. 7a,b,c, respectively, while the symmetric contributions  $(z \leftrightarrow \bar{z})$  originate from the remaining three diagrams. If  $x_1, |x_2| \gg k_\perp^2/s$  then both  $\alpha$  and  $k_\perp^2$  can be neglected in this expression and the factor  $J$  is easily recognized as the  $\gamma^* g \rightarrow V g$  on-shell amplitude

$$J \rightarrow \mathcal{M}_{\gamma^* g \rightarrow V g} \sim \int_0^1 dz \frac{\phi_V(z)}{z \bar{z}}. \quad (3.24)$$

Note that in this case the diagrams in Fig. 7c and Fig. 7f do not contribute. Performing the remaining integration and collecting all factors we recover the result in (3.15) obtained earlier in the Feynman gauge. On the other hand, the contribution of the singularity at

<sup>¶</sup>The singularity at  $x_1 \rightarrow 0$  is in fact irrelevant since the gluon distribution  $\mathcal{F}_\zeta^g(x_1)$  (3.1) vanishes at this point [23], cf. Eq. (3.16).

$x_2 = 0$ , or, equivalently, of the imaginary part of the amplitude requires some attention. First note that the expression for  $J$  vanishes identically when  $x_1 \rightarrow 0$  or  $x_2 \rightarrow 0$ . As a consequence, the  $1/(x_1 x_2)$  factor appearing in Eq. (3.22) does not in fact produce any singularity *in the gauge invariant sum of all Feynman diagrams*. The result of the calculation, therefore, does not depend on a particular prescription to go around the auxiliary singularity in the gluon propagator in the light-cone gauge. Any prescription produces the same result. Since the poles at  $x_2 = 0$  and  $x_1 = 0$  are spurious, we are left with the imaginary parts corresponding to  $+i\epsilon$  prescription in the Feynman propagator in (3.23) and invoking the standard argument with the contour deformation recover the  $x_2 + i\epsilon$  in (3.15). The gauge prescription becomes important, however, if one insists on QCD factorization in each Feynman diagram separately. Consider  $x_2 \rightarrow 0$  and two different prescriptions for the factor  $1/[(k - \zeta p_2)p_1 \pm i\epsilon]$  in the gluon propagator. The first term in (3.23) corresponding to the diagram in Fig. 7a contains a factor  $x_2$  in the numerator and is not affected. In the second term, corresponding to Fig. 7b, one can still take the light-cone limit and neglect  $\alpha$  and  $k_\perp$ . The contribution of this diagram then reads

$$\mathcal{M}_{(b)} \sim \int dx_1 \frac{\mathcal{F}_\zeta^g(x_1)}{x_1(x_2 \pm i\epsilon)} \frac{1}{z}. \quad (3.25)$$

It has both real and imaginary parts and the sign of the imaginary part depends on the gauge prescription. Note that in covariant gauges this ‘crossed box’ diagram has no imaginary part in the physical region. The third contribution in Eq. (3.23) originates from the diagram in Fig. 7c and is more delicate. This contribution vanishes in the ‘naive’ light-cone limit. In the vicinity of the point  $x_2 = 0$  the small factor  $k_\perp^2$  in the numerator is compensated, however, by the small denominator:

$$\mathcal{M}_{(c)} \sim \int dx_1 \frac{\mathcal{F}_\zeta^g(x_1)}{x_1(x_2 \pm i\epsilon)} \frac{1}{z} \frac{k_\perp^2}{[(\alpha + \bar{z})x_2 s - k_\perp^2 + i\epsilon]}. \quad (3.26)$$

At small  $k_\perp^2$  and  $\alpha \sim k_\perp^2/s$  this reduces to

$$\mathcal{M}_{(c)} \sim \int dx_1 \frac{\mathcal{F}_\zeta^g(x_1)}{x_1} \frac{1}{z} \left( -\frac{1}{[x_2 \pm i\epsilon]} + \frac{1}{[x_2 + i\epsilon]} \right). \quad (3.27)$$

We see that first, the gauge poles  $[x_2 \pm i\epsilon]$  indeed cancel in the sum of diagrams in Fig. 7b and Fig. 7c and, second, the diagram in Fig. 7c is equal to zero in the light-cone limit if and only if one chooses the  $+i\epsilon$  prescription for the gauge pole. The reason becomes obvious if one tries to deform the integration contour in  $x_1$  away from the singularity at  $x_1 = \zeta(x_2 = 0)$ , as shown in Fig. 5. If the  $+i\epsilon$  prescription for the gauge pole is used, both the gauge pole and the pole of the quark propagator lie below the real axis. Hence the contour deformation is not obstructed and taking the limit  $k_\perp \rightarrow 0$  we obtain zero, the parton model result for the contribution of this diagram. On the other hand, if the  $-i\epsilon$  prescription is used, the gauge pole appears to be above the real axis and in the  $k_\perp \rightarrow 0$  limit is pinched with the pole of the quark propagator. In this case one cannot move the contour away from the singularity. As the result, the diagram in Fig. 7c acquires a non-zero imaginary part which has no parton model interpretation and, most importantly, is missed in the ‘naive’ calculation when  $k_\perp$  and  $\alpha$  are put to zero at the beginning.

The net outcome of our discussion is the verification of the ansatz in Eq. (3.3) for the leading-order contribution in the strong coupling: One can calculate the hard coefficient function as on-shell  $\gamma^* g \rightarrow Vg$  amplitude, and use the prescription in (3.3) for the definition of the gluon distribution in Eq. (3.1). In order to assemble the all-order proof, one has to show that to arbitrary order in perturbation theory the poles of Feynman propagators corresponding to soft gluon exchanges all lie below the  $x_2$  real axis. The corresponding discussion can be found in [7]. The physical interpretation is that all soft gluon exchanges can be thought of as part of the final state interaction between the outgoing hadrons; they are reduced to eikonal factors that enter the (gauge-invariant) definition of the gluon distribution. Pinching of the singularities in this case cannot occur since initial state soft interactions are not present. The interpretation of the  $\pm i\epsilon$  prescriptions in (3.3) as due to soft final state interactions allows for an alternative derivation of this result, by noticing that the suitable boundary condition for the gluon field in the light-cone gauge is such that [31, 23]

$$A_\mu(y) = p_1^\nu \int_0^\infty G_{\mu\nu}(y + \sigma p_1) e^{-\epsilon\sigma} d\sigma \quad (3.28)$$

with the integration extended to plus infinity in time. We remind that  $p_1$  is the pion momentum. It is easy to check [23] that the ansatz in (3.3) is an immediate consequence of this relation. A still another interpretation of this ansatz is that the amplitude of hard exclusive meson production only has a  $s$ -channel discontinuity in the physical region. Its energy dependence has, therefore, to be a function of  $s + i\epsilon$  which translates to  $\zeta \rightarrow \zeta - i\epsilon$  and  $x_2 \rightarrow x_1 - \zeta + i\epsilon = x_2 + i\epsilon$ , respectively. In any case, we see that the ansatz in (3.3) is specific for the considered process and cannot be taken over for the hard dijet production without a careful analysis. In fact, the very existence of such an ansatz is a consequence of QCD factorization<sup>||</sup>.

### 3.2 Dijet production: Dispersion approach

Since the theoretical status of hard dijet production continues to be controversial [17, 18, 19, 20], in this paper we will present our calculation using two different techniques and show that both lead to the same result. In this section we calculate the imaginary part of the  $\pi \rightarrow 2$  jets scattering amplitude on a quark target in the high energy limit. The imaginary part is interesting in several respects. First, we have found in Sec. 2 that the imaginary part of the quark exchange is affected by the pinch singularities and contains logarithmic end-point divergencies which destroy collinear factorization. Since

---

<sup>||</sup> An instructive example is provided by the process  $Vp \rightarrow \gamma^*(Q^2)p$  where the photon in the final state has positive virtuality. This reaction is similar to electroproduction and can be treated in the same way. In this case, however, the leading-order calculation yields the prescription  $[x_2 - i\epsilon]$ , i.e. opposite to the ansatz in (3.3). The reason is that the soft interaction is in the initial state in this case, and in order to preserve the parton picture one has to use a different gauge condition. Another difference is that the amplitude  $Vp \rightarrow \gamma^*(Q^2)p$  has nonzero dispersive parts in both variables  $s$  and  $Q^2$ . One can check that the contributions of  $s$ -channel singularities all cancel in the light-cone limit with part of the singularities in the  $Q^2$ -channel. Hence one is left with  $Q^2$ -channel singularities alone, and the dependence of the amplitude on  $[x_1 - \zeta - i\epsilon]$  can be understood as the replacement  $Q^2 \rightarrow Q^2 + i\epsilon$ .

Feynman diagrams describing quark and gluon contributions have similar topologies, the same problem is expected for the gluon contribution as well. Second, at high energies the scattering amplitude corresponding to Pomeron exchange is dominated by its imaginary part, so that this contribution is numerically the most important one. Last but not least, the cut diagrams appearing in the calculation of the imaginary part are built of tree-level on-shell scattering amplitudes and their form is strongly constrained by gauge invariance, see below. This simplification has been widely used in the literature in the calculations of high-energy asymptotics of scattering amplitudes starting from [32, 33]. The idea to use this approach for the dijet production was suggested in [18].

The  $s$ -channel discontinuity of the amplitude  $\pi q \rightarrow 2 \text{ jets} + q$  is described by the cut diagrams shown in Fig. 8. They can be grouped into the four gauge-invariant contributions in Fig. 8a-d which differ by the position of the hard gluon that provides the large

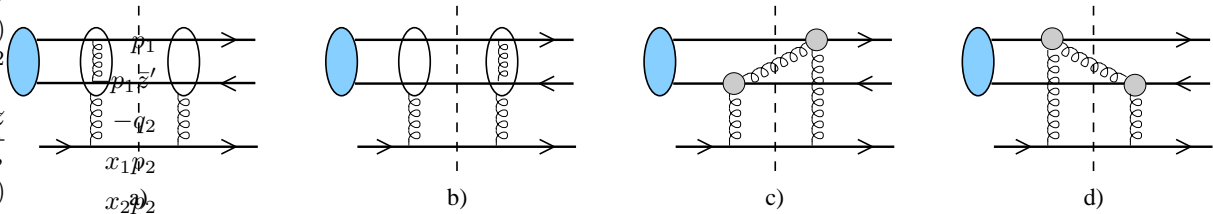


Figure 8: The decomposition of the imaginary part of the amplitude  $\pi q \rightarrow (\bar{q}q)q$  into four gauge-invariant contributions.

momentum transfer to the jets. The corresponding contributions to the imaginary part of the amplitude will be denoted by  $\mathcal{C}_{(a)}$ ,  $\mathcal{C}_{(b)}$ ,  $\mathcal{C}_{(c)}$  and  $\mathcal{C}_{(d)}$ , respectively. For example, in Fig. 8a it is assumed that the hard gluon exchange appears to the left of the cut. This contribution is given by the sum of 10 Feynman diagrams, for further details see our letter [19]. Similarly, the contribution in Fig. 8b is given by the sum of 10 diagrams with the hard gluon exchange appearing to the right of the cut. The two remaining contributions in Fig. 8c and Fig. 8d take into account the possibility of real gluon emission in the intermediate state. The filled circles stand for the effective vertices describing gluon radiation, see Fig. 9. Each of the two contributions in Fig. 8c,d corresponds to a sum of 9 different Feynman diagrams.

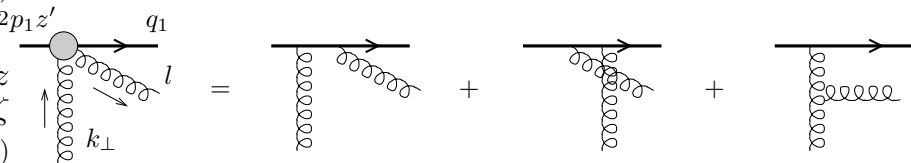


Figure 9: The effective vertex.

At first sight, we have to consider the discontinuity in the invariant mass  $M^2$  of the jets as well. It is easy to check that the corresponding cut diagrams have to have the hard gluon exchange to the right of the cut in order that the transition from the intermediate to the final state corresponds to a physical process. On the other hand, unlike for the  $s$ -discontinuity, the  $t$ -channel gluon lines can be crossed in this case. The two possible cut

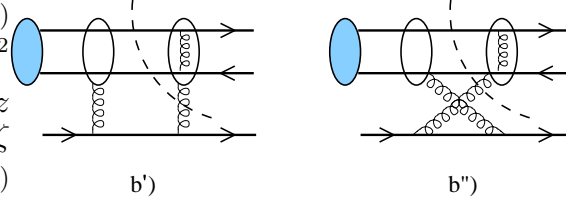


Figure 10: The  $M^2$ -discontinuity of the amplitude  $\pi q \rightarrow (\bar{q}q)q$ .

diagrams are shown in Fig. 10. We denote the corresponding contributions by  $\mathcal{C}_{(b')}$  and  $\mathcal{C}_{(b'')}$ , respectively. They differ by the interchange of the Mandelstam variables  $s$  and  $u$ .

It is known for a long time that at high-energies any amplitude with vacuum quantum numbers exchange in the  $t$ -channel has to be crossing-symmetric, or in other words has positive signature. In our case we are dealing with a two-gluon exchange that grows linearly with energy and consider a one-loop amplitude which adds a logarithm. The crossing symmetry then implies that the contribution to the scattering amplitude of which  $\mathcal{C}_{(b)}$ ,  $\mathcal{C}_{(b')}$  and  $\mathcal{C}_{(b'')}$  are the three nonvanishing dispersion parts in the physical region of the  $s$ -channel has the following schematic structure:

$$\mathcal{M} \sim s \ln \left( \frac{-s}{-M^2} \right) + u \log \left( \frac{-u}{-M^2} \right) + \mathcal{O}(s^0). \quad (3.29)$$

At high energies  $u \simeq -s$  and the above structure implies that the  $s$ -channel and the  $M^2$ -channel discontinuities are related:  $\mathcal{C}_{(b)} = -\mathcal{C}_{(b')}$  and  $\mathcal{C}_{(b')} = -\mathcal{C}_{(b'')}$ . The first equality  $\mathcal{C}_{(b)} = -\mathcal{C}_{(b')}$  which amounts to the cancellation of the  $s$ -channel and  $M^2$ -channel discontinuities is not specific for high energies, but rather a general property of the scaling limit: In so far as the amplitude is a function of the dimensionless ratio  $(-s)/(-M^2)$ , the  $s$ - and  $M^2$ -discontinuities cancel each other identically\*\*. It follows that the total imaginary part of the amplitude  $\pi q \rightarrow (\bar{q}q)q$  in the scaling limit is given by the sum of the three  $s$ -channel cut diagrams in Fig. 8a,c,d and the  $M^2$ -cut diagram with crossed  $t$ -channel gluon lines in Fig. 10b''. However, at high energies the crossing symmetry implies that  $\mathcal{C}_{(b'')} = \mathcal{C}_{(b)}$  and the net result is that the  $M^2$ -discontinuity can be neglected altogether. We are left, therefore, with the set of cut diagrams shown in Fig. 8.

The general strategy of the calculation is the following. As is easily checked by inspection, in any cut diagram two internal lines are on the mass shell. The corresponding two on-shellness conditions fix  $\alpha$  and  $x_1$  variables in the Sudakov parametrisation (3.11) of the gluon momentum and relate the variables  $z'$  and  $x_1$  (see Fig. 1 for the notations) to one other. Since the  $\alpha$  and  $x$ -variables for both gluons are of the order of  $1/s$ , the  $1/k_{1,2}^2$  factors in the propagators of the  $t$ -channel gluons can be approximated by using  $k^2 \simeq -k_\perp^2$ , to the  $\mathcal{O}(1/s)$  accuracy. In this calculation we use the Feynman gauge and perform the usual substitution  $g_{\mu\nu} \rightarrow p_2^\mu p_1^\nu / (p_1 p_2)$  in the numerators of the  $t$ -channel gluon propagators, which is valid to the same accuracy. Using the on-shellness conditions for the contributions in Fig. 8a and Fig. 8b one obtains  $x_1 = \zeta$ ,  $x_2 = 0$ , for any  $z'$ . For Fig. 8d one finds  $x_1 = \zeta z' \bar{z} / (z' - z)$ ,  $x_2 = \zeta z \bar{z}' / (z' - z)$  and  $z' > z$ , where the last condition ensures that

\*\*We have already met with an example of such cancellation for the quark contribution, see the discussion of cut diagrams in Fig. 6(2c-I) and Fig. 6(2c-II).

the energy of the cut gluon is positive. Finally, for the set of cut-diagrams corresponding to Fig. 8c we obtain  $x_1 = \zeta z \bar{z}' / (z - z')$ ,  $x_2 = \zeta z' \bar{z} / (z - z')$  and  $z > z'$ .

After the on-shellness conditions are used, a single integration over the gluons transverse momentum  $k_\perp$  remains:

$$\text{Im } \mathcal{M} \sim \int \frac{d^2 k_\perp}{(k_\perp^2)^2} J_{up}(k_\perp, q_\perp) J_{down}(k_\perp, q_\perp), \quad (3.30)$$

where  $k_\perp^4$  comes from the product of the two gluon propagators.  $J_{up}$  and  $J_{down}$  are dubbed impact factors and stand for the upper and the lower parts of the diagrams in Fig. 8a–d that are connected by the two-gluon exchange. The representation (3.30) is well known [32, 33] from studies of QED scattering at high energies.

Properties of the impact-factors  $J_{up}$  and  $J_{down}$  as a functions of  $k_\perp$  at  $k_\perp \rightarrow 0$  are of crucial importance. Since  $J_{down}$  is the impact-factor of a point-like target quark,  $J_{down}(k_\perp, q_\perp) \sim \text{const.}$  On the other hand,  $J_{up}(k_\perp, q_\perp)$  stands for the scattering of the colorless  $q\bar{q}$  (Fig. 8a–b) or  $q\bar{q}G$  (Fig. 8c–d) state having a transverse size  $\sim 1/q_\perp$  and has to vanish at small  $k_\perp \ll q_\perp$ ,  $J_{up}(k_\perp, q_\perp) \sim k_\perp^2$ , as a consequence of the color neutrality of the quark-antiquark pair: A gluon with a large wave length  $\sim 1/k_\perp$  cannot resolve a color dipole of the small size  $\sim 1/q_\perp$ . Since in our case there are two gluons,  $J_{up}$  is proportional to the product  $k_\perp \cdot k_\perp = k_\perp^2$ <sup>††</sup>. In the opposite limit of large transferred momenta,  $k_\perp \gg q_\perp$ , the two  $t$ -channel gluons are forced to couple to the same parton (quark or gluon) in the upper block in Fig. 8a–d. It follows that at large  $k_\perp$   $J_{up}(k_\perp, q_\perp) \sim \text{const.}$

Taking into account the properties of the impact-factors discussed above, we conclude that the transverse momentum integration in (3.30) diverges logarithmically at small  $k_\perp$  and the integral can be estimated by  $\mathcal{M} \sim \int^{q_\perp^2} dk_\perp^2 / k_\perp^2 \sim \ln q_\perp^2$ , as expected. The region of  $k_\perp^2 > q_\perp^2$  does not produce the large logarithm and can be neglected. Note that the correct small  $k_\perp$  behavior of the impact factors is only recovered in the sum of cut diagrams for the gauge invariant amplitudes  $\mathcal{C}_{(a)}$ ,  $\mathcal{C}_{(b)}$ ,  $\mathcal{C}_{(c)}$  and  $\mathcal{C}_{(d)}$ , but not for each diagram separately.

In addition to the diagrams discussed so far, the amplitude  $\pi q \rightarrow (\bar{q}q)q$  receives a contribution from the three-gluon exchange in the  $t$ -channel. Such terms can be viewed as belonging to the cut diagrams shown in Fig. 8a in which the hard gluon in the blob is attached to the bottom quark line. We have checked that this extra contribution does not contain the large collinear logarithm  $\ln q_\perp^2$  and therefore we neglect it.

The calculation of  $\mathcal{C}_{(d)}$  proceeds as follows. Let  $l^\mu = \alpha_l p_1^\mu + x_l p_2^\mu + l_\perp^\mu$  be the momentum of the (real) gluon in the intermediate state and let  $e^\mu(l)$  be one of the two physical polarization vectors. The two conditions  $(e \cdot p_2) = 0$  and  $(e \cdot l) = 0$  fix the gauge and result in  $e^\mu(l) = e_\perp^\mu + 2p_2^\mu (e_\perp l_\perp) / (\alpha_l s)$ .

The effective vertex corresponding to the sum of the three diagrams in Fig. 9 has the form

$$i \frac{g^2 z (z' - z)}{q_\perp^2 z'} \left[ \frac{1}{z'} (t^l t^a)_{ij} - \frac{1}{z} (t^a t^l)_{ij} \right] \bar{u}(q_1) \left[ \not{p}_2 - 2 \frac{z}{z' - z} (e_\perp b) \right] \frac{\not{p}_2}{s} u(z' p_1). \quad (3.31)$$

Here  $t^l$  and  $t^a$  are the  $SU(3)$  generators. The color indices  $l$  and  $a$  belong to the emitted

---

<sup>††</sup>The  $\mathcal{O}(k_\perp^2)$  behavior can be traced to the gauge invariance of the amplitude, see [33] for the details.

gluon and the  $t$ -channel gluon, respectively. We have also introduced an auxiliary two-dimensional vector  $b^\mu$  defined as:

$$b^\mu = k_\perp^\mu - 2 \frac{(k_\perp q_\perp)}{q_\perp^2} q_\perp^\mu, \quad b^2 = k_\perp^2. \quad (3.32)$$

Note that the effective vertex, in the limit of small  $k_\perp$ , is proportional to  $b \propto k_\perp$ . The constant terms cancel in the gauge invariant sum of the diagrams in Fig. 9.

The second effective vertex in Fig. 8d has a similar form. Combining both of them and performing the sum over the polarizations of the emitted gluon we obtain the impact-factor  $J_{up}^{(d)}$ . Since each effective vertex is proportional to  $k_\perp$ , it follows that  $J_{up}^{(d)} \sim k_\perp^2$ , as expected. The result for the amplitude  $\mathcal{C}_{(d)}$  is obtained using the representation in (3.30). The calculation of  $\mathcal{C}_{(c)}$  is very similar. The result for their sum reads:

$$\begin{aligned} \mathcal{C}_{(c)} + \mathcal{C}_{(d)} = D C_F^2 \int \frac{dk_\perp^2}{k_\perp^2} \int_0^1 dz' \phi_\pi(z') \left( \frac{z \bar{z}}{z' \bar{z}'} + 1 \right) \times \\ \times \left[ \left( \frac{z \bar{z}}{z' \bar{z}'} + 1 \right) + \frac{1}{(N_c^2 - 1)} \left( \frac{z}{z'} + \frac{\bar{z}}{\bar{z}'} \right) \right] \left[ \frac{\Theta(z' - z)}{(z' - z)} + \frac{\Theta(z - z')}{(z - z')} \right], \end{aligned} \quad (3.33)$$

where

$$D = -i s f_\pi \alpha_s^3 \frac{4 \pi^2}{N_c^2 q_\perp^4} \bar{u}(q_1) \gamma_5 \frac{\not{p}_2}{s} v(q_2) \delta_{ij} \delta_{cc'}. \quad (3.34)$$

The color indices  $(i, j)$  correspond to the produced quark-antiquark pair (jets) and  $(c, c')$  stand for the color indices of the target quark in the initial and the final state. The contributions  $\sim \Theta(z' - z)$  and  $\sim \Theta(z - z')$  belong to  $\mathcal{M}_{(d)}$  and  $\mathcal{M}_{(c)}$ , respectively.

For the cut diagrams in Fig. 8a and Fig. 8b we obtain:

$$\begin{aligned} \mathcal{C}_{(a)} = -D C_F^2 \int \frac{dk_\perp^2}{k_\perp^2} \int_0^1 dz' \phi_\pi(z') \left( \frac{\bar{z}}{z'} + \frac{z}{\bar{z}'} \right), \\ \mathcal{C}_{(b)} = D C_F^2 \int \frac{dk_\perp^2}{k_\perp^2} \int_0^1 dz' \frac{\phi_\pi(z')}{z' \bar{z}'} \left[ z \bar{z} \left( \frac{\bar{z}}{z'} + \frac{z}{\bar{z}'} \right) + \frac{1}{(N_c^2 - 1)} \left( \frac{z \bar{z}}{z' \bar{z}'} + 1 \right) \right]. \end{aligned} \quad (3.35)$$

The transverse momentum integrals in (3.33) and (3.35) can be identified with the small  $x$  limit,  $x, \zeta \ll 1$ , of the (perturbative) generalized gluon distributions of a quark defined in Eq. (3.16):  $\mathcal{F}_\zeta^g(x) \simeq \frac{\alpha_s}{\pi} C_F \int dk_\perp^2 / k_\perp^2$ . We obtain, in this approximation [19]

$$\frac{1}{\pi} \text{Im} [i \mathcal{M}_{\text{gluon}}] = s f_\pi \alpha_s^2 \frac{4 \pi^2}{N_c^2 q_\perp^4} \bar{u}(q_1) \gamma_5 \frac{\not{p}_2}{s} v(q_2) \tilde{\mathcal{I}} \delta_{ij} \quad (3.36)$$

with

$$\tilde{\mathcal{I}} = \int_0^1 dz' \phi_\pi(z', \mu^2) \left\{ \left[ C_F \left( \frac{z \bar{z}}{z' \bar{z}'} - 1 \right) \left( \frac{\bar{z}}{z'} + \frac{z}{\bar{z}'} \right) + \frac{1}{2N_c z' \bar{z}'} \left( \frac{z \bar{z}}{z' \bar{z}'} + 1 \right) \right] \mathcal{F}_\zeta^g(\zeta, \mu^2) \right\}$$

$$\begin{aligned}
& + \left( \frac{z\bar{z}}{z'\bar{z}'} + 1 \right) \left[ C_F \left( \frac{z\bar{z}}{z'\bar{z}'} + 1 \right) + \frac{1}{2N_c} \left( \frac{z}{z'} + \frac{\bar{z}}{\bar{z}'} \right) \right] \\
& \times \left[ \frac{\Theta(z' - z)}{(z' - z)} \mathcal{F}_\zeta^g \left( \frac{\zeta z' \bar{z}}{z' - z}, \mu^2 \right) + \frac{\Theta(z - z')}{(z - z')} \mathcal{F}_\zeta^g \left( \frac{\zeta \bar{z}' z}{z - z'}, \mu^2 \right) \right] \Big\}. \tag{3.37}
\end{aligned}$$

The expression in Eq. (3.37) presents the main result of this section. Note that the integrand in (3.37) is singular at  $z' = z$  so that there is a logarithmic enhancement of the contribution of the integration region  $\zeta \ll |z' - z| \ll 1$ . In addition, there is a logarithmic divergence at the end-points  $z' \rightarrow 0$  and  $z' \rightarrow 1$  which signals that the collinear factorization is broken, as expected. In what follows we will discuss the contributions from these regions in some detail. Before doing this, however, in the next section we derive the complete result for the amplitude in the scaling limit (both real and imaginary parts, and including  $\mathcal{O}(1/s)$  corrections) using a different approach.

### 3.3 Dijet production: Factorization and the light-cone limit

Our aim in this section is to derive the complete result for the leading-order contribution to the kernel  $T_H^g(z, z', x_1, x_2)$  such that

$$\mathcal{M}_{\text{gluon}} = \frac{4\pi^2 \alpha_s^2 s i f_\pi}{N_c^2 q_\perp^4} \sqrt{1 - \zeta} \bar{u}(q_1) \gamma_5 \frac{\not{p}_2}{s} v(q_2) \delta_{ij} \int_0^1 dz' \phi_\pi(z') \int_0^1 dx_1 \mathcal{F}_\zeta^g(x_1) T_{\text{gluon}}(z, z', x_1, x_2), \tag{3.38}$$

cf. Eq. (1.2). For high energies,  $\zeta \rightarrow 0$ , we expect to recover in this way the result of the direct calculation of the imaginary part given in (3.37).

We will mainly be concerned with the singularity structure of  $T_{\text{gluon}}(z, z', x_1, x_2)$  at  $x_2 \rightarrow 0$ . The singularity structure at  $x_1 \rightarrow 0$  can, in principle, be found from similar considerations. This is in fact not necessary since it can be established using the crossing symmetry  $T_{\text{gluon}}(z, z', x_1, x_2) = T_{\text{gluon}}(z, z', -x_2, -x_1)$  that corresponds to the interchange of  $s$ - and  $u$ -channels for the corresponding pion-gluon amplitude. Apart from this issue, the calculation of  $T_{\text{gluon}}(z, z', x_1, x_2)$  is straightforward and can most easily be done by considering pion scattering from on-shell transversely polarized gluons, cf. [20]. For the simpler case of hard exclusive production of vector mesons we have argued in Sect. 3.1 that the light-cone calculation (with on-shell gluons) is actually sufficient since the singularity structure in Eq. (3.15) can be restored using the prescription (3.3) in the definition of the off-forward gluon distribution (3.1). One way to understand this result was that for hard exclusive production of vector mesons it is possible to choose an axial (light-cone) gauge in such a way that gauge singularities of the  $t$ -channel gluons and causal singularities of Feynman propagators lie on the same side of the integration contour in  $x_1$  so that there are no pinches in the Glauber region. In the present case, a similar simplification is not expected since soft gluon exchanges occur both in the initial and in the final state.

The complete set of relevant Feynman diagrams is shown in Fig. 11. For 20 out of in total 31 existing diagrams, Fig. 11(1-20), it is kinematically possible that the  $t$ -channel gluon with vanishing momentum fraction  $x_2$  couples either to the initial or to the final on-shell quark lines. The corresponding quark propagators produce a singularity in the

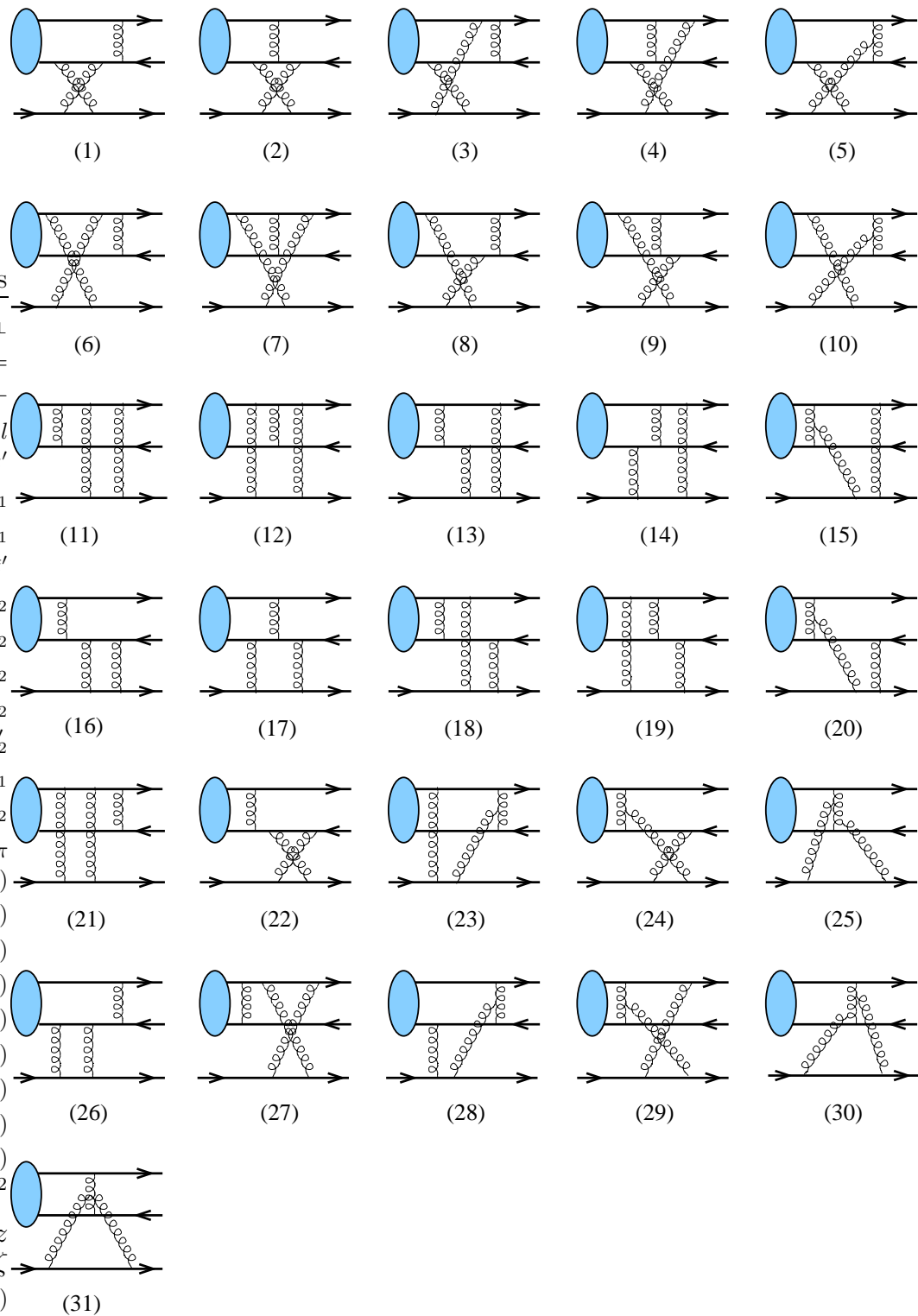


Figure 11: The complete set of Feynman diagrams for the two-gluon exchange contribution to the process  $\pi q \rightarrow (\bar{q}q)q$  to the leading order in the strong coupling.

$x_2 \rightarrow 0$  limit. In particular, in the 5 diagrams in Fig. 11(11-15) where the soft gluon is attached to the outgoing quark, the quark propagator is

$$1/[(q_1 + k - \zeta p_2)^2 + i\epsilon] = 1/[(z + \alpha)(x_1 - \zeta z)s - (q_\perp + k_\perp)^2 + i\epsilon] \rightarrow 1/[zs(x_2 + i\epsilon)] \quad (3.39)$$

in the limit  $\alpha, k_\perp \rightarrow 0$ . Similarly, in the 5 diagrams in Fig. 11(16-20) where the gluon is attached to the outgoing antiquark, one obtains

$$1/[(q_2 + k - \zeta p_2)^2 + i\epsilon] = 1/[(\bar{z} + \alpha)(x_1 - \zeta \bar{z})s - (q_\perp + k_\perp)^2 + i\epsilon] \rightarrow 1/[\bar{z}s(x_2 + i\epsilon)] \quad (3.40)$$

in the same limit. However, in the 5 diagrams in Fig. 11(1-5) where the soft gluon is emitted by the ingoing antiquark, the denominator of the quark propagator is

$$1/[(\bar{z}'p_1 - k + \zeta p_2)^2 + i\epsilon] = 1/[(\bar{z}' - \alpha)(\zeta - x_1)s - k_\perp^2 + i\epsilon] \rightarrow 1/[-\bar{z}'s(x_2 - i\epsilon)] \quad (3.41)$$

and similar for the diagrams in Fig. 11(6-10)

$$1/[(z'p_1 - k + \zeta p_2)^2 + i\epsilon] = 1/[(z' - \alpha)(\zeta - x_1)s - k_\perp^2 + i\epsilon] \rightarrow 1/[-z's(x_2 - i\epsilon)]. \quad (3.42)$$

We see that both types of singularities are produced,  $(x_2 \pm i\epsilon)$ , depending on whether the soft interaction occurs in the initial or in the final state [29]. As a consequence, it is not possible to choose an axial gauge in which the light-cone limit exists for each Feynman diagram separately.

For definiteness, let us define the light-cone gauge in the same way as this was convenient for hard exclusive production of vector mesons,  $1/x_2 \rightarrow 1/(x_2 + i\epsilon)$ . In this case the diagrams with soft interaction in the final state Fig. 11(11-20) and the diagrams that are non-singular in the  $x_2 \rightarrow 0$  limit Fig. 11(21-31) can be calculated in the light-cone limit, with on-shell  $t$ -channel gluons, and the result multiplied by the gluon distribution (3.1) using the prescription in (3.3). On the other hand, in the diagrams with soft interaction in the initial state Fig. 11(1-10) the integration contour over  $x_1$  will be pinched. We can calculate their contribution by deforming the integration contour in the same direction as for the other diagrams  $x_2 = x_1 - \zeta + i\epsilon$ , and adding the contribution of the pole of the quark propagator (3.41) and (3.42). In what follows we refer to these two contributions as ‘naive’ light-cone  $T_i^{\text{LC}}$  and pole  $T_i^{\text{pole}}$  contributions, respectively. The subscript ‘ $i$ ’ numerates the diagrams according to Fig. 11. The additional pole contributions are present (with our gauge choice) in the diagrams in Fig. 11(1-10) so that

$$T_{\text{gluon}}(z, z', x_1, x_2) = T^{\text{LC}} + T^{\text{pole}} = \sum_{i=1}^{31} T_i^{\text{LC}} + \sum_{i=1}^{10} T_i^{\text{pole}}. \quad (3.43)$$

$T^{\text{LC}}$  can be calculated as the gauge-invariant on-shell pion-gluon scattering amplitude, times the gauge factor (3.3)

$$T^{\text{LC}} = \frac{\zeta}{(x_1 - i\epsilon)(x_2 + i\epsilon)} \sum_{i=1}^{31} \mathcal{A}_i^{\pi g \rightarrow (\bar{q}q)g} \quad (3.44)$$

where  $\mathcal{A}_i$  correspond to the upper parts of the diagrams in Fig. 11, not including the target quark and the propagators of the  $t$ -channel gluons. Since  $\mathcal{A}^{\pi g \rightarrow (\bar{q}q)g} = \sum_{i=1}^{31} \mathcal{A}_i^{\pi g \rightarrow (\bar{q}q)g}$  is the

amplitude of a physical process, it is gauge invariant and can be calculated in any gauge. In the Feynman gauge we find

$$\begin{aligned}
\mathcal{A}_1 &= C_F \frac{\bar{z}z^2}{z'\bar{z}'} , \quad \mathcal{A}_2 = -\frac{1}{2N_c} \frac{z^2(x_1 - z\zeta)}{z'\bar{z}'[x_1 - i\epsilon]} , \quad \mathcal{A}_{16} = C_F \frac{z^2(2\zeta\bar{z} - x_1)}{z'[x_2 + i\epsilon]} , \\
\mathcal{A}_3 &= -C_F \frac{z^2\bar{z}^2\zeta}{z'\bar{z}'[(z' - z)x_1 - z'\bar{z}\zeta + i\epsilon]} , \quad \mathcal{A}_4 = -\frac{1}{2N_c} \frac{z^2\bar{z}^2\zeta^2}{\bar{z}'[x_1 - i\epsilon][(z' - z)x_1 - z'\bar{z}\zeta + i\epsilon]} , \\
\mathcal{A}_5 &= \frac{N_c}{4} \frac{\bar{z}z^2(2x_1 + \zeta(1 - z' - 2z))}{z'\bar{z}'[(z' - z)x_1 - z'\bar{z}\zeta + i\epsilon]} , \quad \mathcal{A}_{20} = -\frac{N_c}{4} \frac{z^2(2x_1^2 - 3\zeta x_1\bar{z} + \zeta^2\bar{z}(3 - 4z))}{z'[x_2 + i\epsilon][(z' - z)x_1 - z'\bar{z}\zeta + i\epsilon]} , \\
\mathcal{A}_{31} &= -N_c \frac{z\bar{z}}{z'\bar{z}'} , \quad \mathcal{A}_{25} = -\frac{N_c}{2} \frac{z\bar{z}(\zeta x_1(4 + z' - z) - 4x_1^2 - \zeta^2(2 - 5z + zz' + 4z^2))}{z'\bar{z}'\zeta[(z' - z)x_1 - z'\bar{z}\zeta + i\epsilon]} , \\
\mathcal{A}_{18} &= C_F \frac{z\bar{z}\zeta(\zeta^2z\bar{z} - (x_1 - \zeta\bar{z})^2)}{[x_1 - i\epsilon][x_2 + i\epsilon][(z' - z)x_1 - z'\bar{z}\zeta + i\epsilon]} . \tag{3.45}
\end{aligned}$$

The remaining contributions are given by the replacements

$$\begin{aligned}
\mathcal{A}_1(z, z', x_1, x_2) &= \mathcal{A}_6(\bar{z}, \bar{z}', x_1, x_2) = \mathcal{A}_{26}(z, z', -x_2, -x_1) = \mathcal{A}_{21}(\bar{z}, \bar{z}', -x_2, -x_1) , \\
\mathcal{A}_2(z, z', x_1, x_2) &= \mathcal{A}_7(\bar{z}, \bar{z}', x_1, x_2) = \mathcal{A}_{17}(z, z', -x_2, -x_1) = \mathcal{A}_{12}(\bar{z}, \bar{z}', -x_2, -x_1) , \\
\mathcal{A}_4(z, z', x_1, x_2) &= \mathcal{A}_9(\bar{z}, \bar{z}', x_1, x_2) = \mathcal{A}_{14}(z, z', -x_2, -x_1) = \mathcal{A}_{19}(\bar{z}, \bar{z}', -x_2, -x_1) , \\
\mathcal{A}_5(z, z', x_1, x_2) &= \mathcal{A}_{10}(\bar{z}, \bar{z}', x_1, x_2) = \mathcal{A}_{28}(z, z', -x_2, -x_1) = \mathcal{A}_{23}(\bar{z}, \bar{z}', -x_2, -x_1) , \\
\mathcal{A}_{16}(z, z', x_1, x_2) &= \mathcal{A}_{11}(\bar{z}, \bar{z}', x_1, x_2) = \mathcal{A}_{22}(z, z', -x_2, -x_1) = \mathcal{A}_{27}(\bar{z}, \bar{z}', -x_2, -x_1) , \\
\mathcal{A}_{20}(z, z', x_1, x_2) &= \mathcal{A}_{15}(\bar{z}, \bar{z}', x_1, x_2) = \mathcal{A}_{24}(z, z', -x_2, -x_1) = \mathcal{A}_{29}(\bar{z}, \bar{z}', -x_2, -x_1) , \\
\mathcal{A}_{25}(z, z', x_2, x_1) &= \mathcal{A}_{30}(z, z', -x_2, -x_1) , \quad \mathcal{A}_3(z, z', x_1, x_2) = \mathcal{A}_8(z, z', -x_2, -x_1) , \\
\mathcal{A}_{18}(z, z', x_1, x_2) &= \mathcal{A}_{13}(z, z', -x_2, -x_1) . \tag{3.46}
\end{aligned}$$

For the sum of all diagrams we obtain

$$\begin{aligned}
T^{\text{LC}}(z, z', x_1, x_2) &= C_F \left( \frac{\bar{z}}{z'} + \frac{z}{\bar{z}'} \right) \left( \frac{\zeta}{[x_1 - i\epsilon]^2} + \frac{\zeta}{[x_2 + i\epsilon]^2} - \frac{\zeta}{[x_1 - i\epsilon][x_2 + i\epsilon]} \right) \\
&\quad + \left( \frac{z\bar{z}}{z'\bar{z}'} + 1 \right) \left[ C_F \left( \frac{z\bar{z}}{z'\bar{z}'} + 1 \right) + \frac{1}{2N_c} \left( \frac{z}{z'} + \frac{\bar{z}}{\bar{z}'} \right) \right] \\
&\quad \times \left( \frac{1}{[(z - z')x_1 - z\bar{z}'\zeta + i\epsilon]} + \frac{1}{[(z' - z)x_2 - z\bar{z}'\zeta + i\epsilon]} \right) \\
&\quad - \left[ C_F \frac{z\bar{z}}{z'\bar{z}'} \left( \frac{\bar{z}}{z'} + \frac{z}{\bar{z}'} \right) + \frac{1}{2N_c z'\bar{z}'} \left( \frac{z\bar{z}}{z'\bar{z}'} + 1 \right) \right] \frac{\zeta}{[x_1 - i\epsilon][x_2 + i\epsilon]} . \tag{3.47}
\end{aligned}$$

Taking the imaginary part of (3.47) we reproduce the answer for the imaginary part of the coefficient function obtained in Ref. [20]<sup>††</sup>.

<sup>††</sup> In order to make the comparison it is necessary to take into account that the answer given in [20] is rewritten in a different form using the symmetry  $\phi_\pi(z) = \phi_\pi(1 - z)$  of the pion distribution amplitude.

As explained above, this is not the whole story, however, and one has to add the pole contributions. For example, consider the diagram in Fig. 11(3). In the notation of Sect. 3.1 we obtain the corresponding contribution as

$$\begin{aligned} \mathcal{M}_3 = & -g^6 f_\pi \sqrt{1-\zeta} \frac{C_F^2}{8N_c^2} \int \frac{d^4 k}{(2\pi)^4} \int_0^1 dz' \phi_\pi(z') \mathcal{R}_{\mu_1\mu_2}^{\text{LC}} N_{\nu_1\nu_2}(k + z' p_1 - q_1) \quad (3.48) \\ & \times \bar{u}(q_1) \gamma_{\nu_1} \frac{(z' \not{p}_1 + \not{k})}{(z' p_1 + k)^2 + i\epsilon} \gamma_{\mu_1} \gamma_5 \not{p}_1 \gamma_{\mu_2} \frac{(\not{k} - \zeta \not{p}_2 - \bar{z}' \not{p}_1)}{(k - \zeta p_2 - \bar{z}' p_1)^2 + i\epsilon} \gamma_{\nu_2} v(q_2), \end{aligned}$$

where  $\mathcal{R}_{\mu_1\mu_2}^{\text{LC}}$  is defined in Eq. (3.19) and  $N_{\nu_1\nu_2}(k + z' p_1 - q_1)$  is the nominator of the hard gluon propagator in axial gauge. In the present case only the first two terms in Eq. (3.20) contribute and according to our procedure we choose the prescription  $1/x_2 \rightarrow 1/[x_2 + i\epsilon]$  in the corresponding factor in Eq. (3.19). This singularity is due to gauge fixing and is pinched with the quark propagator  $[(k - \zeta p_2 - \bar{z}' p_1)^2 + i\epsilon]$ , cf. (3.41). Although at the end we have to isolate the quark propagator pole contribution, it is convenient to rewrite the gauge pole as

$$\frac{1}{[x_2 + i\epsilon]} = \frac{1}{[x_2 - i\epsilon]} - (2\pi i) \delta(x_2) \quad (3.49)$$

and find the corresponding two contributions to (3.48) separately

$$\mathcal{M}_3 = \mathcal{M}_3^a + \mathcal{M}_3^b \quad (3.50)$$

as an intermediate step.

Calculation of the first term,  $\mathcal{M}_3^a$ , is straightforward since poles of the quark propagator and  $1/[x_2 - i\epsilon]$  do not pinch. One can neglect  $k_\perp$  and  $\alpha$  in the integrand of (3.48) everywhere except in  $\mathcal{R}_{\mu_1\mu_2}^{\text{LC}}$ . The integral of  $\mathcal{R}_{\mu_1\mu_2}^{\text{LC}}$  over  $\alpha$  and  $k_\perp$  reproduces the generalized gluon distribution, cf. (3.21), and gets factored out. The remainder gives the contribution to the coefficient function (in the light-cone gauge)

$$T_3^a = C_F \frac{z^2 \bar{z}^2 \zeta^2 [\zeta(2z' - z) - x_1]}{z' \bar{z}' x_1 [x_2 - i\epsilon] [(z' - z)x_1 - \zeta z' \bar{z} + i\epsilon] (x_1 - \zeta \bar{z})}. \quad (3.51)$$

The factor  $(x_1 - \zeta \bar{z})$  in the denominator of the above expression originates from the hard gluon exchange propagator in the light cone gauge, the factor  $N_{\nu_1\nu_2}(k + z' p_1 - q_1)$  in Eq. (3.48).

In the second term,  $\mathcal{M}_3^b$ , we use the  $\delta$ -function to put  $x_1 \rightarrow \zeta$  and need to expand the quark propagators in Eq. (3.48) in the limit  $k_\perp \rightarrow 0$  and  $\alpha \sim k_\perp^2/s$ . To the required accuracy

$$\begin{aligned} \mathcal{M}_3^b = & \frac{4\pi^2 \alpha_s^2 s i f_\pi}{N_c^2 q_\perp^4} \sqrt{1-\zeta} \bar{u}(q_1) \gamma_5 \frac{\not{p}_2}{s} v(q_2) \delta_{ij} \int_0^1 dz' \phi_\pi(z') \quad (3.52) \\ & \times \frac{C_F}{2\pi} \int \frac{dx_1 d(\alpha s) dk_\perp^2 \delta(x_2)(2-\zeta)}{[(\alpha s)\zeta - k_\perp^2 + i\epsilon] [(\alpha s)(\zeta-1) - k_\perp^2 + i\epsilon]} \left( \frac{C_F \bar{z}^3}{\bar{z}'^2} + \mathcal{O}(k_\perp^2) \right). \end{aligned}$$

The integration over  $\alpha$  produces the expression which can be identified with the perturbative leading-order generalized gluon distribution of a quark at the point  $\mathcal{F}_\zeta^q(x_1 = \zeta)$ , cf. Eq. (3.16). The corresponding coefficient function takes the form

$$T_3^b = (2\pi i)\delta(x_2)C_F \frac{\bar{z}^3}{\bar{z}'^2}. \quad (3.53)$$

As the final step, we go from  $1/[x_2 - i\epsilon]$  in eq. (3.51) to  $1/[x_2 + i\epsilon]$  using (3.49). The result equals the contribution of this diagram in the ‘naive’ light-cone limit,  $T_3^{\text{LC}}$ , and the extra terms  $\sim \delta(x_2)$  correspond to the ‘pole’ contribution  $T_3^{\text{pole}}$  in the sense of Eq. (3.43). We obtain

$$T_3^{\text{LC}} = C_F \frac{z^2 \bar{z}^2 \zeta^2 [\zeta(2z' - z) - x_1]}{z' \bar{z}' x_1 [x_2 + i\epsilon] [(z' - z)x_1 - \zeta z' \bar{z} + i\epsilon] (x_1 - \zeta \bar{z})}, \quad (3.54)$$

and

$$T_3^{\text{pole}} = (2\pi i)\delta(x_2)C_F \frac{\bar{z}^2(1+z)}{z' \bar{z}'}. \quad (3.55)$$

Note that in difference to the expressions collected in (3.45) the result in (3.54) is obtained in the light-cone gauge.

Calculation of the other diagrams is similar. We obtain

$$\begin{aligned} T_1^{\text{pole}} &= (2\pi i)\delta(x_2)C_F \frac{\bar{z}z^2}{z' \bar{z}'}, \\ T_2^{\text{pole}} &= -(2\pi i)\delta(x_2) \frac{1}{2N_c} \frac{\bar{z}z^2(2z' - 1)}{z' \bar{z}'} - \delta(x_2) \frac{1}{2N_c} \eta \frac{\bar{z}z^2}{z'}, \\ T_4^{\text{pole}} &= -(2\pi i)\delta(x_2) \frac{1}{2N_c} \frac{z\bar{z}^2(3 - 2z')}{\bar{z}'^2} + \delta(x_2) \frac{1}{2N_c} \eta \frac{z\bar{z}^2}{\bar{z}'}, \\ T_5^{\text{pole}} &= (2\pi i)\delta(x_2) \frac{N_c}{2} \frac{\bar{z}(z' - z^2 - 1)}{z' \bar{z}'^2} + \delta(x_2) \frac{N_c}{2} \eta \frac{z\bar{z}(2z - 1)}{2z' \bar{z}'}, \end{aligned} \quad (3.56)$$

and

$$\begin{aligned} T_6^{\text{pole}}(z, z') &= T_1^{\text{pole}}(\bar{z}, \bar{z}'), & T_7^{\text{pole}}(z, z') &= T_2^{\text{pole}}(\bar{z}, \bar{z}'), & T_8^{\text{pole}}(z, z') &= T_3^{\text{pole}}(\bar{z}, \bar{z}'), \\ T_9^{\text{pole}}(z, z') &= T_4^{\text{pole}}(\bar{z}, \bar{z}'), & T_{10}^{\text{pole}}(z, z') &= T_5^{\text{pole}}(\bar{z}, \bar{z}'). \end{aligned} \quad (3.57)$$

In these expressions

$$\eta = \frac{2\zeta}{(2 - \zeta)} \int \frac{d(\alpha s)(k_\perp^2 + 2(\alpha s)(1 - \zeta))}{[(\alpha s)\zeta - k_\perp^2 + i\epsilon][(\alpha s)(\zeta - 1) - k_\perp^2 + i\epsilon]}. \quad (3.58)$$

The corresponding contributions originate from the last term in Eq. (3.20) and at first sight are dangerous because an additional factor  $\alpha$  in the numerator of (3.58) makes the integral divergent at  $\alpha \rightarrow \infty$ . This difficulty is, however, spurious since the terms  $\sim \eta$  actually cancel in the sum of all ten diagrams. For the sum of pole terms we obtain

$$T^{\text{pole}} = \sum_{i=1, \dots, 10} T_i^{\text{pole}} = -(2\pi i)\delta(x_2) \left[ C_F \frac{z\bar{z}}{z' \bar{z}'} \left( \frac{\bar{z}}{z'} + \frac{z}{\bar{z}'} \right) + \frac{1}{2N_c z' \bar{z}'} \left( \frac{z\bar{z}}{z' \bar{z}'} + 1 \right) \right], \quad (3.59)$$

and the final answer for the gluon coefficient function (3.38) can be written as

$$\begin{aligned}
T_{\text{gluon}}(z, z', x_1, x_2) = & C_F \left( \frac{\bar{z}}{z'} + \frac{z}{\bar{z}'} \right) \left( \frac{\zeta}{[x_1 - i\epsilon]^2} + \frac{\zeta}{[x_2 + i\epsilon]^2} - \frac{\zeta}{[x_1 - i\epsilon][x_2 + i\epsilon]} \right) \\
& + \left( \frac{z\bar{z}}{z'\bar{z}'} + 1 \right) \left[ C_F \left( \frac{z\bar{z}}{z'\bar{z}'} + 1 \right) + \frac{1}{2N_c} \left( \frac{z}{z'} + \frac{\bar{z}}{\bar{z}'} \right) \right] \\
& \times \left( \frac{1}{[(z - z')x_1 - z\bar{z}'\zeta + i\epsilon]} + \frac{1}{[(z' - z)x_2 - z\bar{z}'\zeta + i\epsilon]} \right) \quad (3.60) \\
& - \left[ C_F \frac{z\bar{z}}{z'\bar{z}'} \left( \frac{\bar{z}}{z'} + \frac{z}{\bar{z}'} \right) + \frac{1}{2N_c z'\bar{z}'} \left( \frac{z\bar{z}}{z'\bar{z}'} + 1 \right) \right] \frac{\zeta}{[x_1 + i\epsilon][x_2 - i\epsilon]}.
\end{aligned}$$

We see that, as we already discussed before, in this expression there are terms with different prescriptions for the poles at  $x_1 = 0, x_2 = 0$ . In particular, in comparison to the light-cone result in (3.47), there are different  $\pm i\epsilon$  prescriptions in the last line.

The corresponding imaginary part is

$$\begin{aligned}
\mathcal{I} \equiv & \int_0^1 dz' \phi_\pi(z', \mu^2) \int_0^1 dx_1 \mathcal{F}_\zeta^g(x_1) \left[ -\frac{1}{\pi} \text{Im} T_{\text{gluon}}(z, z', x_1, x_2) \right] \\
= & \int_0^1 dz' \phi_\pi(z', \mu^2) \left\{ \left[ C_F \left( \frac{z\bar{z}}{z'\bar{z}'} - 1 \right) \left( \frac{\bar{z}}{z'} + \frac{z}{\bar{z}'} \right) + \frac{1}{2N_c z'\bar{z}'} \left( \frac{z\bar{z}}{z'\bar{z}'} + 1 \right) \right] \mathcal{F}_\zeta^g(\zeta, \mu^2) \right. \\
& + \left( \frac{z\bar{z}}{z'\bar{z}'} + 1 \right) \left[ C_F \left( \frac{z\bar{z}}{z'\bar{z}'} + 1 \right) + \frac{1}{2N_c} \left( \frac{z}{z'} + \frac{\bar{z}}{\bar{z}'} \right) \right] \\
& \times \left[ \frac{\Theta(z' - z)}{(z' - z)} \mathcal{F}_\zeta^g \left( \frac{\zeta z' \bar{z}}{z' - z}, \mu^2 \right) + \frac{\Theta(z - z')}{(z - z')} \mathcal{F}_\zeta^g \left( \frac{\zeta \bar{z}' z}{z - z'}, \mu^2 \right) \right] \\
& \left. + C_F \left( \frac{\bar{z}}{z'} + \frac{z}{\bar{z}'} \right) \frac{\zeta}{2} [\mathcal{F}_\zeta^{g'}(\zeta + 0, \mu^2) + \mathcal{F}_\zeta^{g'}(\zeta - 0, \mu^2) - \mathcal{F}_\zeta^{g'}(0, \mu^2)] \right\}. \quad (3.61)
\end{aligned}$$

In the approximation that only the (large) imaginary part of the amplitude is taken into account, the differential cross section summed over the polarizations and the color of quark jets is given by

$$\frac{d\sigma_{\pi \rightarrow 2 \text{jets}}}{dq_\perp^2 dt dz} = \frac{\alpha_s^4 f_\pi^2 \pi^3}{8N_c^3 q_\perp^8} |\mathcal{I}|^2. \quad (3.62)$$

The factorization scale  $\mu^2$  has to be of order of the transverse momentum of the exchanged gluon.

The expressions in (3.60) and (3.61) present the main result of this paper. The expression for the imaginary part in (3.61) indeed reproduces the result in (3.37) apart from the extra last term containing a derivative of the gluon distribution. Using the explicit expression for the perturbative gluon distribution function of a quark in Eq. (3.16) it is easy to check that the derivative term is of order  $\mathcal{O}(\zeta)$  and this is the reason why it was absent in the first calculation.

Note also that  $T^{\text{pole}}$  given in Eq. (3.59) is nothing else but the  $M^2$ -channel discontinuity  $\mathcal{C}_{(b'')}$  given by the crossed diagram in Fig. 10:

$$DC_F \frac{\pi}{\alpha_s} \int dz' \phi_\pi(z') \int dx_1 \mathcal{F}_\zeta^g(x_1) \left[ -\frac{1}{\pi} \text{Im } T^{\text{pole}} \right] = 2\mathcal{C}_{(b'')} \simeq 2\mathcal{C}_{(b)}, \quad (3.63)$$

cf. Eq. (3.35), up to  $\mathcal{O}(\zeta)$  corrections. The imaginary part corresponding to the ‘naive’ light-cone limit is given therefore by the expression  $\tilde{\mathcal{I}}^{\text{LC}} \sim \mathcal{C}_{(a)} - \mathcal{C}_{(b)} + \mathcal{C}_{(c)} + \mathcal{C}_{(d)}$ , i.e. reversing the sign of the contribution in Fig. (8)b.

### 3.4 Discussion

The leading end-point behavior of the coefficient function  $T_{\text{gluon}}(z, z', x_1, x_2)$  (3.60) at  $z' \rightarrow 0$  and  $z' \rightarrow 1$  is given by the following expressions:

$$\begin{aligned} T_{\text{gluon}}|_{z' \rightarrow 0} &\rightarrow -(2\pi i) \frac{z\bar{z}}{z'^2} \left( C_F \bar{z} + \frac{1}{2N_c} \right) [\delta(x_1) + \delta(x_2)], \\ T_{\text{gluon}}|_{z' \rightarrow 1} &\rightarrow -(2\pi i) \frac{z\bar{z}}{\bar{z}'^2} \left( C_F z + \frac{1}{2N_c} \right) [\delta(x_1) + \delta(x_2)]. \end{aligned} \quad (3.64)$$

Since  $\mathcal{F}_\zeta^g(x)$  vanishes at  $x = 0$  [23], only the terms  $\sim \delta(x_2)$  contribute. Note that the leading  $1/z'^2$ ,  $1/\bar{z}'^2$  asymptotics is imaginary, it comes entirely from the term which we denoted  $T^{\text{pole}}$ , see Eq. (3.59). The contribution of  $T^{\text{LC}}$  is at most  $\mathcal{O}(1/z')$ , or  $\mathcal{O}(1/\bar{z}')$ , see also [20]. Eqs. (3.64) have to be compared with Eqs. (2.13), (2.14) for the quark contribution. Similar to the latter case, the collinear factorization is violated due to the pinching of  $M^2$ -channel and  $s$ -channel singularities in the Glauber region. Summing the both contributions in Eq. (3.64) and using the symmetry of the pion distribution amplitude we obtain [19]

$$\mathcal{I} \Big|_{\text{end-points}} = \left( N_c + \frac{1}{N_c} \right) z\bar{z} \int_0^1 dz' \frac{\phi_\pi(z', \mu^2)}{z'^2} \mathcal{F}_\zeta^g(\zeta, \mu^2). \quad (3.65)$$

Since  $\phi_\pi(z') \sim z'$  at  $z' \rightarrow 0$ , the integral over  $z'$  diverges logarithmically. Remarkably, the integral containing the pion distribution amplitude does not involve any  $z$ -dependence. Therefore, the longitudinal momentum distribution of the jets in the nonfactorizable contribution is calculable and, as it turns out, has the shape of the asymptotic pion distribution amplitude  $\phi_\pi^{\text{as}}(z) = 6z\bar{z}$ . The corresponding physical process is the following. The limit  $z' \rightarrow 1$  corresponds to a kinematics in which one quark carries the entire momentum of the pion. The fast quark radiates a hard gluon which carries the fraction  $(1-z)$  of quark momentum. This radiation is perturbative and is described by the effective vertex (3.31) at  $z' = 1$ . In the final step the hard gluon transfers its entire longitudinal and transverse momentum to the quark jet, and emits a soft antiquark which interacts nonperturbatively with the target proton and the pion remnant. It follows that the divergent logarithm in  $\int \phi_\pi(z')/z'^2$  is of the form  $\ln q_\perp^2/\mu_{\text{IR}}^2$  where  $\mu_{\text{IR}}$  is related to the average transverse momentum of the quarks inside the pion. It is possible that in the case of scattering from a heavy

nucleus  $\mu_{\text{IR}}$  may grow as  $\sim A^{1/3}$  because of color filtering. On the other hand, it is likely that the modified factorization approach of [26] can be developed and applied to coherent diffraction as well. A detailed discussion of these possibilities goes beyond the tasks of this paper. The other important integration region is the one when  $\zeta \ll |z' - z| \ll 1$ , i.e. when the longitudinal momentum fraction carried by the quark is close (for high energies) to that of the quark jet in the final state. The enhancement of this region comes from the (small) denominator  $1/(z' - z)$  which is present in the contributions in Fig. 8c,d with real gluon emission in the intermediate state. The logarithmic integral  $\int dz'/|z - z'| \sim \ln s$  is nothing but the usual energy logarithm that accompanies each extra gluon in the gluon ladder. Its appearance is due to the fact the the gluon in Fig. 8c,d can be emitted in a broad rapidity interval and is not constrained to the pion fragmentation region. To logarithmic accuracy we can simplify the integrand in (3.37) by assuming  $z' = z$  everywhere except for the small denominators and the argument of the gluon distribution, to get

$$\mathcal{I}\Big|_{\zeta \ll |z' - z| \ll 1} = 4N_c \phi_\pi(z) \int_z^1 \frac{dz'}{z' - z} \mathcal{F}_\zeta^g(\zeta \frac{z\bar{z}}{z' - z}, q_\perp^2) \simeq 4N_c \phi_\pi(z) \int_\zeta^1 \frac{dy}{y} \mathcal{F}_\zeta^g(y, q_\perp^2). \quad (3.66)$$

For a flat gluon distribution  $\mathcal{F}_\zeta^g(y) \sim \text{const}$  at  $y \rightarrow 0$ , and the integration gives  $\text{const} \cdot \ln 1/\zeta$  which is the above mentioned energy logarithm. Note that the color factors combine to produce  $C_A = N_c$  signaling that the relevant Feynman diagrams in Fig. 8c,d are those with a three-gluon coupling. Moreover, the factor  $2N_c/y$  appearing in (3.66) can be interpreted as the relevant limit of the DGLAP gluon splitting function [6]

$$q_\perp^2 \frac{\partial}{\partial q_\perp^2} \mathcal{F}_\zeta^g(x = \zeta, q_\perp^2) = \frac{\alpha_s}{2\pi} \int_\zeta^1 dy P_\zeta^{gg}(\zeta, y) \mathcal{F}_\zeta^g(y, q_\perp^2) \simeq \frac{\alpha_s}{2\pi} \int_\zeta^1 dy \frac{2N_c}{y} \mathcal{F}_\zeta^g(y, q_\perp^2). \quad (3.67)$$

The quantity on the l.h.s. of (3.67) defines what can be called the unintegrated generalized gluon distribution and the physical meaning of Eqs. (3.66) and (3.67) is that in the region  $z' \sim z$  hard gluon exchange can be viewed as a large transverse momentum part of the gluon distribution in the proton, cf. [17]. This contribution is proportional to the pion distribution amplitude  $\phi_\pi(z, q_\perp^2)$  and contains the enhancement factor  $\ln 1/\zeta \sim \ln s/q_\perp^2$ .

## 4 Numerical Analysis

Since collinear factorization does not hold, the numerical analysis presented below has to be considered as semiquantitative. We will use the simplest prescription to regularize the infrared divergence of the end-point contribution by imposing an explicit cutoff on the quark momentum fraction in the pion

$$\int_0^1 dz' \rightarrow \int_{\mu_{\text{IR}}^2/q_\perp^2}^{1 - \mu_{\text{IR}}^2/q_\perp^2} dz' \quad (4.1)$$

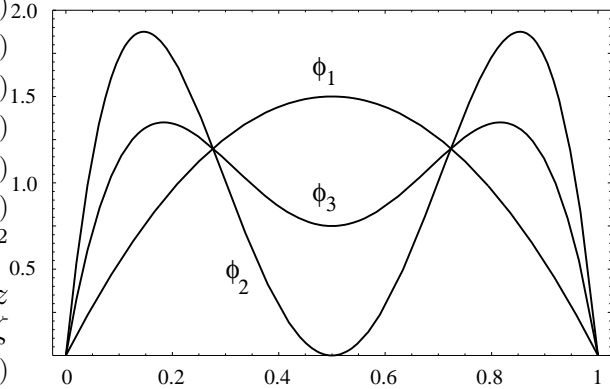


Figure 12: Different models for the pion distribution amplitude, see Eq. (4.2).

with  $\mu_{\text{IR}} = 500$  MeV. We use parametrizations of the generalized quark and gluon parton distributions by Freund and McDermott [35] that are based on the new MRST2001 leading-order forward distributions [36], see Appendix A, and the following trial pion distribution amplitudes:

$$\begin{aligned}\phi_1(z) &= \phi_\pi^{\text{as}}(z) = 6z(1-z), \\ \phi_2(z) &= \phi_\pi^{\text{CZ}}(z, \mu = 0.5 \text{ GeV}) = 30z(1-z)(1-2z)^2, \\ \phi_3(z) &= \phi_\pi^{\text{CZ}}(z, \mu = 2 \text{ GeV}) = 15z(1-z)[0.20 + (1-2z)^2],\end{aligned}\quad (4.2)$$

see Fig. 12. The first expression in (4.2) is the asymptotic distribution amplitude at large scales [2, 3], the second is the Chernyak-Zhitnitsky model [34] and the third is the Chernyak-Zhitnitsky model evolved to the typical scales  $\mu \sim q_\perp = 2$  GeV probed by the E791 experiment [14, 15].  $\phi_1(z)$  and  $\phi_2(z)$  have very different shape and can be considered as two extreme cases. Our aim is to find out whether this difference can give rise to sizeable effects in the momentum fraction distribution of the jets.

Different contributions to imaginary and real parts of the amplitude of the hard dijet production at  $s = 1000$  GeV $^2$  and  $q_\perp = 2$  GeV from the nucleon target for the two extreme choices of the pion distribution amplitudes are plotted in Fig. 13 and Fig. 14. The normalization corresponds to Eqs. (B.5), (B.6), see Appendix B where we collect all the necessary expressions. It is seen that both the imaginary and the real part of the amplitude are dominated by the contribution of the generalized gluon distribution. The singlet quark contribution is less than 25%, and the contributions of  $u$ -quark annihilation and the  $d$ -quark exchange are negligible. In [21] the quark contribution was found to be as important as the gluon one. One reason for the difference is that we use a more realistic parametrization for the quark distributions in our analysis. The second, more important reason, is that our result for the imaginary part of the gluon contribution contains an additional non-factorizable term, the last line in Eq. (B.8), that is related with the discontinuity of the amplitude in the  $M^2$ -channel. This additional contribution is large and constitutes approximately one half of the total result for  $\text{Im}J_{\text{gluon}}$ . Note also that the momentum fraction dependence of  $\text{Im}J_{\text{gluon}}$  deviates considerably from the shape of the pion distribution amplitude. This means that the large-energy approximation in

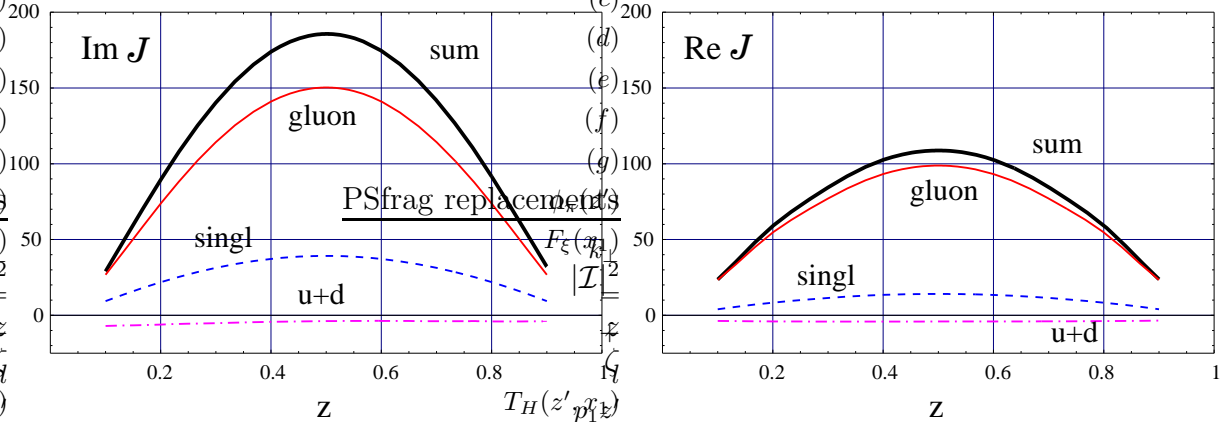


Figure 13: Different contributions to imaginary (left) and real (right) parts of the amplitude of the hard dijet production at  $s = 1000$  GeV $^2$  and  $q_\perp = 2$  GeV from the proton target, assuming the asymptotic pion distribution amplitude  $\phi_\pi(z) = \phi_1(z)$ , Eq. (4.2). The normalization corresponds to Eqs. (B.5), (B.6). Shown are: the gluon contribution (thin solid curve), the quark-singlet contribution (dashed curve) and the  $u$  and  $d$ -quark contributions (dash-dotted curve). In addition, the sum of all contributions is shown by the thick solid curve.

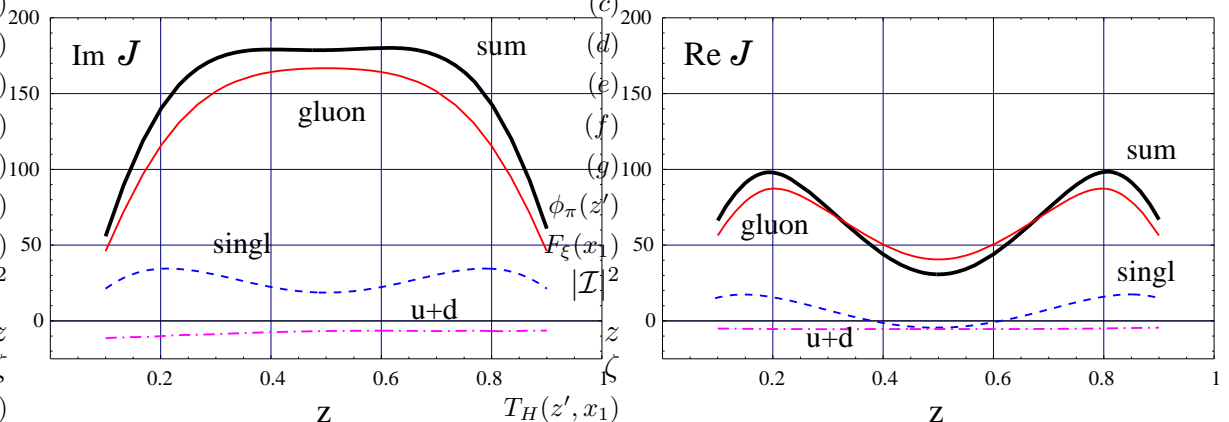


Figure 14: The same as in Fig 13, but with the pion distribution amplitude  $\phi_\pi(z) = \phi_2(z)$  (4.2) corresponding to the Chernyak-Zhitnitsky model at a low normalization point.

Eq. (3.66), where  $\phi_\pi(z)$  enters as an overall factor, is not adequate in the energy range of the E791 experiment.

The real part of the amplitude is significant. The ratio  $\text{Re}/\text{Im}$  is not much smaller than unity and depends both on the assumed shape of the pion distribution amplitude and the jet momentum fraction. Qualitatively, the  $\text{Re}/\text{Im}$  ratio can be estimated using the Gribov-Migdal formula [37]

$$\frac{\text{Re } \mathcal{M}(s)}{\text{Im } \mathcal{M}(s)} = \frac{\pi}{2} \frac{d}{d \ln s} \ln \frac{\text{Im} \mathcal{M}(s)}{s}. \quad (4.3)$$

In our case, the amplitude is roughly proportional to the value of the generalized gluon distribution at the point  $x_1 = \zeta$ ,  $\mathcal{M} \sim \zeta^{-1} \mathcal{F}_\zeta^g(\zeta)$ , and in the relevant kinematic range

$$\mathcal{F}_\zeta^g(\zeta) \simeq 0.52 \zeta^{-0.43}, \quad (4.4)$$

cf. Appendix A. This gives  $\text{Re} \mathcal{M}/\text{Im} \mathcal{M} \sim 0.43 \cdot \pi/2 \simeq 2/3$ , in rough agreement with Figs. 13,14. The large real part is a yet another indication that the energy of E791 experiment is not sufficiently high to consider the process as a diffractive one, mediated by the pomeron exchange.

The discussion in this paper has so far tacitly assumed a nucleon target. For nuclei, one extra effect to be taken into account is the longitudinal momentum transfer that is cut off by the nuclear form factor:

$$\frac{d\sigma_{\pi A \rightarrow q\bar{q}A}}{dq_\perp^2 dz} \sim \frac{d\sigma_{\pi N \rightarrow q\bar{q}N}}{dq_\perp^2 dz} \cdot F_A^2[m^2 \zeta^2], \quad (4.5)$$

where  $\zeta = q_\perp^2/z\bar{z}s$ , cf. (1.3),  $F_A[t] = \exp[-1/6R_A^2 t]$  and  $R_A$  is the mean square radius of the nucleus. We use  $R_A = 5.27$  fm for platinum [14]. In principle, one also has to take into account that the calculated initial momentum fraction distributions at the quark level are modified by nonperturbative hadronization corrections and effects due to the experimental acceptance. These effects lead to a certain broadening of the jet distributions compared to the quark ones, as illustrated in Fig. 2 in Ref. [14]. For simplicity, we ignore them in what follows. We also ignore a tiny QED contribution of Coulomb scattering, calculated in [38].

The comparison of the calculated dijet momentum fraction distribution with the data [14] in the transverse momentum range  $1.5 \leq q_\perp \leq 2.5$  GeV is presented in Fig. 15. The two solid curves correspond to the first two choices of the pion distribution amplitudes in Eq. (4.2) — asymptotic and “two-humped”, respectively. The dashed curve corresponds to the Chernyak-Zhitnitsky model evolved to the scale  $\mu = 2$  GeV. The overall normalization is arbitrary, but is the same for all three choices of the distribution amplitude. It is seen that experimental uncertainties do not allow for the separation between the distribution amplitudes  $\phi_1(z)$  and  $\phi_3(z)$  while the extreme choice  $\phi_2(z)$  (see (4.2) and Fig. 12) is not favored. This general conclusion is in agreement with the analysis in [21].

Finally, one should not forget that the calculation involves a major uncertainty in the choice of the infrared cutoff parameter in the integration over the quark momentum fraction in the pion, Eq. (4.1). Our choice  $\mu_{\text{IR}} = 500$  MeV corresponds to  $z'_{\min} = 1 - z'_{\max} = 0.0625$ . The sensitivity to the IR cutoff is illustrated in Fig. 16 where in addition to our

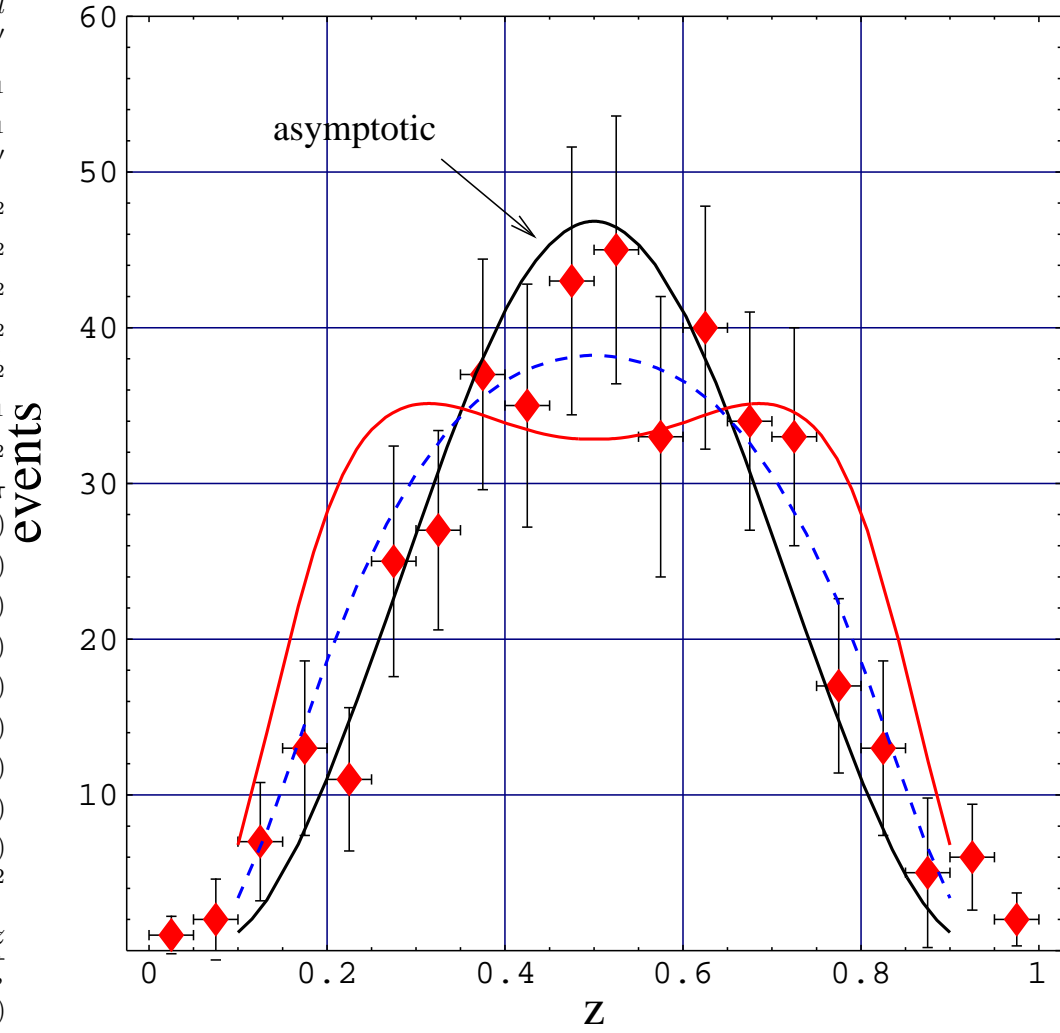


Figure 15: The longitudinal momentum fraction distribution of the dijets with  $1.5 \leq q_\perp \leq 2.5$  GeV from the platinum target [14]. The two solid curves show the calculations with the two extreme pion distribution amplitudes in Eq. (4.2) — asymptotic and “two-humped”, respectively. The dashed curve corresponds to the Chernyak-Zhitnitsky model evolved to the scale  $\mu = 2$  GeV. The overall normalization (the same for all curves) is arbitrary.

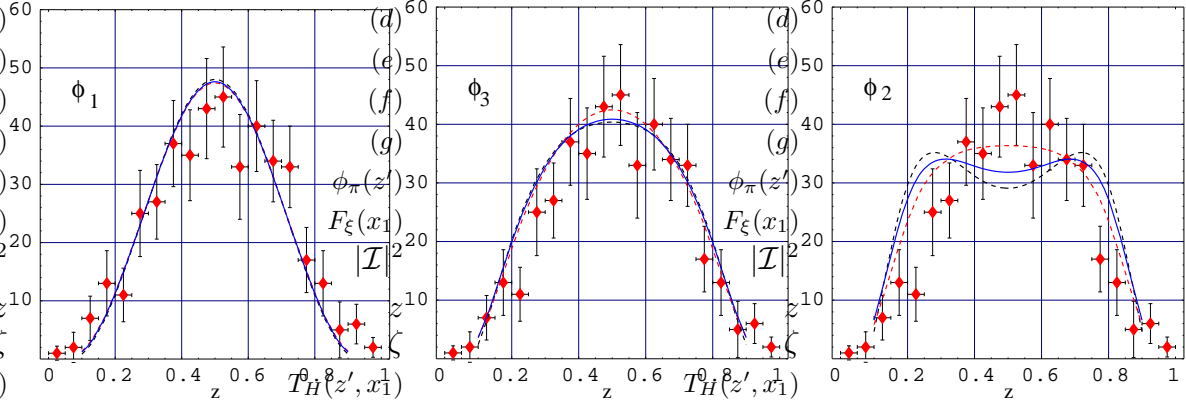


Figure 16: Sensitivity of QCD predictions for the shape of the dijet momentum fraction distribution to the choice of the infrared cutoff for the three different pion distribution amplitudes in Eq. (4.2). The solid curves are calculated with  $z'_{\min} = 0.0625$ , the two dashed curves with  $z'_{\min} = 0.0306$  and  $z'_{\min} = 0.09$ , respectively. The normalization is adjusted to give the same integrated cross section in all cases. The data points are from [14].

“standard” choice (solid curves) we present calculations using  $\mu_{\text{IR}} = 350$  MeV ( $z'_{\min} = 0.0306$ ) and  $\mu_{\text{IR}} = 600$  MeV ( $z'_{\min} = 0.09$ ), shown by dashed curves, for the three trial pion distribution amplitudes. The normalization of curves in Fig. 16 is adjusted to give the same integrated cross section in all cases. We see that for the asymptotic pion distribution function  $\phi_1(z)$  there is no effect at all (within the line thickness), the uncertainty is small for  $\phi_3(z)$ , but more significant for  $\phi_2(z)$ . It is worth while to mention that the well-known strong scale dependence of the gluon distribution at small  $x$  (large energies) by itself leads to an effective suppression of the end-point contribution as compared to the factorizable part of the cross section. Indeed, the end-point contributions effectively correspond to large transverse distances and hence involve a (smaller) gluon distribution at low scales. This effect can be taken into account using the momentum fraction dependent factorization scale  $\mu_F^2 \sim q_\perp^2(z'z')/(z\bar{z})$ , which may present an attractive alternative to the explicit cutoff. It is discussed in our letter [19] and yields results that are qualitatively similar to the calculation presented above.

## 5 Conclusions

We have presented a calculation of the leading contribution to the cross section of pion diffraction dissociation into two jets with large transverse momenta, originating from a hard gluon exchange. Our main result is that collinear factorization is violated. In technical terms, the problem is due to pinching of singularities between soft gluon (and quark) interactions in the initial and in the final state. We have given a detailed analysis of this phenomenon using different techniques, and also explained how the structure of these singularities interferes with gauge prescriptions of the  $t$ -channel gluon propagators. Final expressions for the numerous contributions to the amplitude are collected in Appendix B, where in difference to the main text we use Ji’s conventions [24] for the generalized parton

distributions. Using a realistic set of the generalized parton distributions [35] we find that the coherent dijet production is dominated by the gluon contribution. We also find that the real part of the amplitude is quite sizeable and cannot be neglected.

It happens that the non-factorizable soft contribution to the dijet cross section imitates the shape of the asymptotic pion distribution amplitude. This implies that the dijet production is unlikely to yield fully quantitative constraints on the distribution amplitude. On the other hand, if one accepts that the pion distribution is close to its asymptotic form, as strongly suggested by the CLEO measurement [16] of the  $\gamma\gamma^*\pi$  transition form factor, then it appears that the QCD calculation explains the E791 data on the momentum fraction distributions of dijets very well. We find that the nonfactorizable contribution is suppressed compared to the leading contribution by a logarithm of energy so that for very large energies, in the double logarithmic approximation  $\ln q_\perp^2 \ln \zeta$ , collinear factorization is restored. This limit is achieved for energies about two orders of magnitude larger than the energy in the E791 experiment.

The calculation presented in this work does not address specific nuclear effects, apart from the minor correction of the dijet distribution due to the nuclear form factor. For factorizable contributions of small transverse distances the dijet longitudinal momentum distribution is not expected to exhibit any significant  $A$ -dependence. The place where nuclear effects can play a rôle is by making the infrared cutoff introduced in (4.1)  $A$ -dependent. Indeed, it is plausible to assume that  $\mu_{\text{IR}}^2$  rises with the atomic number, e.g.  $\sim A^{1/3}$ , and hence nonfactorizable contributions become numerically suppressed due to color filtering of configurations with a large transverse size. The corresponding calculation goes beyond the scope of this paper.

A short comparison with other approaches is in order. Our calculation is close in spirit to [20, 21] although the conclusions are different. A detailed explanation of the differences is given in the text. In short, the point is that we do not assume the light-cone dominance of the cross section from the beginning, but examine the light-cone limit carefully and argue that the approximation used in [20, 21] breaks down for Glauber gluons (and quarks). In the double logarithmic approximation our result in (3.66) is similar to [17] obtained using different methods. We, therefore, agree with the interpretation suggested in [17] that in the true diffraction limit, for very large energies, the dijet production can be considered as a probe of the hard component of the pomeron. We note, however, that this interpretation breaks down beyond the double logarithmic approximation and is not sufficient for the energy region of the E791 experiment. Finally, we have to mention an approach to coherent diffraction suggested in [18] that attributes hard dijets to a hard component of the pion wave function as in the original Brodsky-Lepage approach [2]. This technique is interesting since it is most directly related to the classical view on diffraction [9], but apparently complicated for the discussion of factorization. The general argumentation in [18] appears to be in contradiction with our explicit calculations. To our point of view, the coherent states formalism of Refs. [30] can be useful in this context.

## Acknowledgments

We are grateful to V. Chernyak for the correspondence related to the papers [20, 21] and to G. Korchemsky, B. Pire, A. Radyushkin and O. Teryaev for discussions. Our special thanks are due to A. Freund for providing us with the code for the generalized parton distributions. The work of D.I. was supported by the Alexander von Humboldt Foundation.

## Appendices

### A Generalized parton distributions in symmetric notation

In the current literature two different sets of the generalized (off-forward, skewed etc.) parton distributions are used, as introduced in Refs. [23, 24], respectively. Our discussion in the text assumed the definitions Eqs. (2.1) and (3.1) that correspond to the conventions of [23]. The transition to the notations of [24] is straightforward and corresponds to the redefinition

$$\begin{aligned} (1+\xi)\mathcal{H}_q(y, \xi) &= \mathcal{F}_\zeta^q(x) - \mathcal{F}_\zeta^{\bar{q}}(\zeta - x)\Theta(-1 + \zeta \leq x \leq \zeta), \\ (1+\xi)\mathcal{H}_g(y, \xi) &= \mathcal{F}_\zeta^g(x) + \mathcal{F}_\zeta^g(\zeta - x)\Theta(-1 + \zeta \leq x \leq \zeta). \end{aligned} \quad (\text{A.1})$$

The two sets of variables  $(x, \zeta)$  and  $(y, \xi)$  are related according to

$$\begin{aligned} y &= \frac{x - \zeta/2}{1 - \zeta/2}, & \xi &= \frac{\zeta/2}{1 - \zeta/2}; \\ x &= \frac{y + \xi}{1 + \xi}, & \zeta &= \frac{2\xi}{1 + \xi}. \end{aligned} \quad (\text{A.2})$$

$y$  varies in the interval  $-1 \leq y \leq 1$ .

Rewriting of our results to the notations of [24] is straightforward. Using the crossing symmetry of the gluon coefficient function  $T_{\text{gluon}}(x) = T_{\text{gluon}}(\zeta - x)$ , one can easily verify that

$$\mathcal{M}_{\text{gluon}} \sim \int_0^1 dx \mathcal{F}_\zeta^g(x) T_{\text{gluon}}(x) = \frac{1}{2} \int_{-1}^1 dy \mathcal{H}_g(y, \xi) T_{\text{gluon}}\left(\frac{y + \xi}{1 + \xi}\right). \quad (\text{A.3})$$

Note that the gluon distribution  $\mathcal{H}_g(y, \xi)$  is a symmetric function,  $\mathcal{H}_g(y, \xi) = \mathcal{H}_g(-y, \xi)$ .

In the quark case we have

$$\mathcal{M}_{\text{quark}} \sim \int_0^1 dx \left[ \mathcal{F}_\zeta^q(x) T_q(x) + \mathcal{F}_\zeta^{\bar{q}}(x) T_{\bar{q}}(x) \right] = \int_{-1}^1 dy \mathcal{H}_q(y, \xi) T_q\left(\frac{y + \xi}{1 + \xi}\right), \quad (\text{A.4})$$

since quark and antiquark coefficient functions are related,  $T_q(x) = -T_{\bar{q}}(\zeta - x)$ , cf. (2.9).

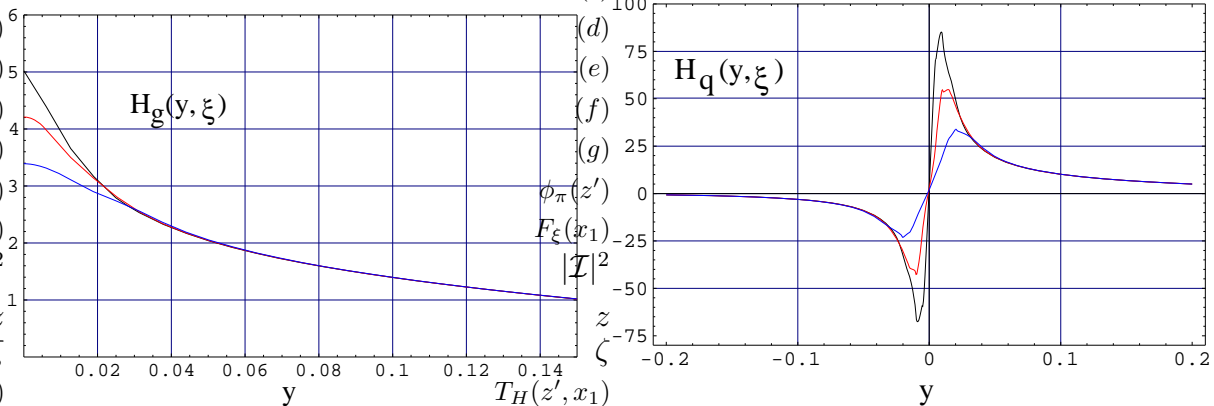


Figure 17: Gluon (left) and flavor-singlet quark (right) generalized parton distributions, for three different values of the asymmetry parameter  $\xi = 0.008$ ,  $\xi = 0.012$  and  $\xi = 0.02$  (from top to bottom) at the scale  $\mu_F = 2$  GeV, [35], based on the LO MRST2001 parametrization [36].

In the numerical calculations in this paper we have used the set of leading-order parton distributions by Freund and McDermott based on the LO MRST2001 parametrization [36], see Fig. 17.

## B Summary of Results

Here we collect our final results. The hard coherent dijet production differential cross section is equal to

$$\frac{d\sigma_{\pi \rightarrow q\bar{q}}}{dq_\perp^2 dt dz} \Big|_{t=0} = \frac{\alpha_s^4 f_\pi^2 \pi^3}{8 N_c^3 q_\perp^8} (1 + \xi)^2 |\mathcal{J}|^2, \quad (\text{B.5})$$

where we separate the quark and gluon contributions

$$\mathcal{J} = -\frac{1}{\pi} (J_{\text{gluon}} + J_{\text{quark}}). \quad (\text{B.6})$$

The gluon contribution reads

$$\begin{aligned} J_{\text{gluon}} = & \frac{1}{2} \int_{-1}^1 dy \mathcal{H}_g(y, \xi) \int_0^1 dz' \phi_\pi(z') \left\{ C_F \left( \frac{\bar{z}}{z'} + \frac{z}{\bar{z}'} \right) \left( \frac{2\xi}{(y + \xi - i\epsilon)^2} + \frac{2\xi}{(y - \xi + i\epsilon)^2} \right) \right. \\ & + \left( \frac{z\bar{z}}{z'\bar{z}'} + 1 \right) \left[ \left( C_F \left( \frac{z\bar{z}}{z'\bar{z}'} + 1 \right) + \frac{1}{2N_c} \left( \frac{z}{z'} + \frac{\bar{z}}{\bar{z}'} \right) \right) \right. \\ & \times \left( \frac{1}{y(z - z') - \xi(z\bar{z}' + z'\bar{z}) + i\epsilon} + \frac{1}{y(z' - z) - \xi(z\bar{z}' + z'\bar{z}) + i\epsilon} \right) \\ & - \left( C_F \left( \frac{\bar{z}}{z'} + \frac{z}{\bar{z}'} \right) + \frac{1}{2N_c z' \bar{z}'} \right) \frac{2\xi}{(y + \xi - i\epsilon)(y - \xi + i\epsilon)} \Big] \\ & \left. - (2\pi i) \left( C_F \frac{z\bar{z}}{z'\bar{z}'} \left( \frac{\bar{z}}{z'} + \frac{z}{\bar{z}'} \right) + \frac{1}{2N_c z' \bar{z}'} \left( \frac{z\bar{z}}{z'\bar{z}'} + 1 \right) \right) (\delta(y + \xi) + \delta(y - \xi)) \right\}. \quad (\text{B.7}) \end{aligned}$$

The contribution in the last line of (B.7) corresponds to the pole contribution discussed in the text; the rest of the terms correspond to the naive light-cone limit  $\xi \rightarrow \xi - i\epsilon$ . The corresponding imaginary and real parts are

$$\begin{aligned}
-\frac{1}{\pi} \text{Im} (J_{\text{gluon}}) = & \int_0^1 dz' \phi_\pi(z') \left[ C_F \left( \frac{\bar{z}}{z'} + \frac{z}{\bar{z}'} \right) 2\xi \mathcal{H}'_g(\xi, \xi) \right. \\
& + \left( \frac{z\bar{z}}{z'\bar{z}'} + 1 \right) \left\{ \left( C_F \left( \frac{z\bar{z}}{z'\bar{z}'} + 1 \right) + \frac{1}{2N_c} \left( \frac{z}{z'} + \frac{\bar{z}}{\bar{z}'} \right) \right) \frac{\mathcal{H}_g(\frac{\xi(z\bar{z}'+z'\bar{z})}{|z'-z|}, \xi)}{|z'-z|} \right. \\
& - \left. \left( C_F \left( \frac{\bar{z}}{z'} + \frac{z}{\bar{z}'} \right) + \frac{1}{2N_c z' \bar{z}'} \right) \mathcal{H}_g(\xi, \xi) \right\} \\
& \left. + 2 \left( C_F \frac{z\bar{z}}{z'\bar{z}'} \left( \frac{\bar{z}}{z'} + \frac{z}{\bar{z}'} \right) + \frac{1}{2N_c z' \bar{z}'} \left( \frac{z\bar{z}}{z'\bar{z}'} + 1 \right) \right) \mathcal{H}_g(\xi, \xi) \right]. \quad (\text{B.8})
\end{aligned}$$

and

$$\begin{aligned}
\text{Re} (J_{\text{gluon}}) = & \int_0^1 dz' \int_0^1 dy \phi_\pi(z') \left\{ C_F \left( \frac{\bar{z}}{z'} + \frac{z}{\bar{z}'} \right) \left( \frac{2\xi \mathcal{H}_g(y, \xi)}{(y + \xi)^2} \right. \right. \\
& + \frac{2\xi(\mathcal{H}_g(y, \xi) - \mathcal{H}_g(\xi, \xi) - (y - \xi)H'(\xi, \xi))}{(y - \xi)^2} \Big) \\
& + \left( \frac{z\bar{z}}{z'\bar{z}'} + 1 \right) \left[ \left( C_F \left( \frac{z\bar{z}}{z'\bar{z}'} + 1 \right) + \frac{1}{2N_c} \left( \frac{z}{z'} + \frac{\bar{z}}{\bar{z}'} \right) \right) \right. \\
& \times 2\xi(z\bar{z}' + z'\bar{z}) \frac{\mathcal{H}_g(y, \xi) - \mathcal{H}_g(\frac{\xi(z\bar{z}'+z'\bar{z})}{|z'-z|}, \xi)}{y^2(z' - z)^2 - \xi^2(z\bar{z}' + z'\bar{z})^2} \\
& - \left. \left( C_F \left( \frac{\bar{z}}{z'} + \frac{z}{\bar{z}'} \right) + \frac{1}{2N_c z' \bar{z}'} \right) \frac{2\xi(\mathcal{H}_g(y, \xi) - \mathcal{H}_g(\xi, \xi))}{y^2 - \xi^2} \right] \Big) \\
& + \int_0^1 dz' \phi_\pi(z') \left\{ C_F \left( \frac{\bar{z}}{z'} + \frac{z}{\bar{z}'} \right) \left( 2\xi \mathcal{H}'_g(\xi, \xi) \ln \left( \frac{1 - \xi}{\xi} \right) - \frac{2\mathcal{H}_g(\xi, \xi)}{1 - \xi} \right) \right. \\
& + \left( \frac{z\bar{z}}{z'\bar{z}'} + 1 \right) \left[ \left( C_F \left( \frac{z\bar{z}}{z'\bar{z}'} + 1 \right) + \frac{1}{2N_c} \left( \frac{z}{z'} + \frac{\bar{z}}{\bar{z}'} \right) \right) \right. \\
& \times \frac{\mathcal{H}_g(\frac{\xi(z\bar{z}'+z'\bar{z})}{|z'-z|}, \xi)}{|z' - z|} \ln \left( \left| \frac{|z' - z| - \xi(z\bar{z}' + z'\bar{z})}{|z' - z| + \xi(z\bar{z}' + z'\bar{z})} \right| \right) \\
& - \left. \left( C_F \left( \frac{\bar{z}}{z'} + \frac{z}{\bar{z}'} \right) + \frac{1}{2N_c z' \bar{z}'} \right) \mathcal{H}_g(\xi, \xi) \ln \left( \frac{1 - \xi}{1 + \xi} \right) \right] \Big) \Big\}, \quad (\text{B.9})
\end{aligned}$$

where  $\mathcal{H}'_g(\xi, \xi) = (d/dy)\mathcal{H}_g(y, \xi)|_{y=\xi}$ . Although the gluon distribution is generally not an analytic function at  $y = \xi$ , we have checked that the first derivative exists for the leading

order perturbative distribution (3.16) and one can prove that it also exists in the formal  $\mu_F \rightarrow \infty$  limit.

For the quark contribution we distinguish between the flavor-singlet contribution mediated by the hard two-gluon exchange in the  $t$ -channel, and the separate contributions of  $u$  and  $d$  quarks:

$$J_{\text{quark}} = \frac{2\xi z \bar{z}}{1 + \xi} (J_{\text{singl}} + J_u + J_d). \quad (\text{B.10})$$

We also introduce the flavor-singlet quark distribution

$$\mathcal{H}_q(y, \xi) = \sum_{p=u,d,s} \mathcal{H}_p(y, \xi). \quad (\text{B.11})$$

For the flavor-singlet contribution we obtain

$$J_{\text{singl}} = \int_{-1}^1 dy \mathcal{H}_q(y, \xi) \int_0^1 dz' \phi_\pi(z') C_F \left( \frac{z \bar{z}}{z' \bar{z}'} + 1 \right) \frac{2y}{y^2(z - z')^2 - \xi^2(z \bar{z}' + z' \bar{z})^2 + i\epsilon}, \quad (\text{B.12})$$

so that

$$\begin{aligned} -\frac{1}{\pi} \text{Im} (J_{\text{singl}}) &= \int_0^1 dz' \phi_\pi(z') C_F \left( \frac{z \bar{z}}{z' \bar{z}'} + 1 \right) \frac{1}{(z - z')^2} \\ &\times \left[ \mathcal{H}_q \left( \frac{\xi(z \bar{z}' + z' \bar{z})}{|z' - z|}, \xi \right) - \mathcal{H}_q \left( \frac{-\xi(z \bar{z}' + z' \bar{z})}{|z' - z|}, \xi \right) \right] \end{aligned} \quad (\text{B.13})$$

and

$$\begin{aligned} \text{Re} (J_{\text{singl}}) &= \int_{-1}^1 dy \int_0^1 dz' \phi_\pi(z') C_F \left( \frac{z \bar{z}}{z' \bar{z}'} + 1 \right) \frac{2y \left( \mathcal{H}_q(y, \xi) - \mathcal{H}_q \left( \frac{\text{sign}(y)\xi(z \bar{z}' + z' \bar{z})}{|z - z'|}, \xi \right) \right)}{y^2(z - z')^2 - \xi^2(z \bar{z}' + z' \bar{z})^2} \\ &+ \int_0^1 dz' \phi_\pi(z') C_F \left( \frac{z \bar{z}}{z' \bar{z}'} + 1 \right) \ln \left( \left| \frac{(z - z')^2 - \xi^2(z \bar{z}' + z' \bar{z})^2}{\xi^2(z \bar{z}' + z' \bar{z})^2} \right| \right) \\ &\times \left[ \frac{\mathcal{H}_q \left( \frac{\xi(z \bar{z}' + z' \bar{z})}{|z - z'|}, \xi \right) - \mathcal{H}_q \left( \frac{-\xi(z \bar{z}' + z' \bar{z})}{|z' - z|}, \xi \right)}{(z - z')^2} \right]. \end{aligned} \quad (\text{B.14})$$

For the flavor-nonsinglet contributions we obtain

$$\begin{aligned} J_u &= 2C_F \int_{-1}^1 dy \mathcal{H}_u(y, \xi) \int_0^1 dz' \phi_\pi(z') \left[ C_F \left( \frac{z(2 - z)}{\bar{z} \bar{z}'(y + \xi - i\epsilon)} + \frac{z}{z'(y - \xi + i\epsilon)} \right) \right. \\ &\left. + \frac{1}{2N_c} \left( \frac{z}{\bar{z} \bar{z}'^2(y + \xi - i\epsilon)} + \frac{(z - \bar{z}')^3}{z' \bar{z}'^2 \bar{z}(y(\bar{z}' - z) - \xi(z \bar{z}' + \bar{z} \bar{z}')) + i\epsilon} \right) \right] \end{aligned}$$

$$\begin{aligned}
& + \frac{1}{\bar{z}(y(z' - z) - \xi(z\bar{z}' + z'\bar{z}) + i\epsilon)} + \frac{z\bar{z}}{z'\bar{z}'^2(y(z - z') - \xi(z\bar{z}' + z'\bar{z}) + i\epsilon)} \Big) \\
& - (2\pi i) \left( C_F \frac{z(2-z)}{\bar{z}\bar{z}'} + \frac{1}{2N_c} \frac{z}{\bar{z}\bar{z}'} \right) \delta(y + \xi) \Big], \tag{B.15}
\end{aligned}$$

$$\begin{aligned}
-\frac{1}{\pi} \text{Im}(J_u) = & 2C_F \int_0^1 dz' \phi_\pi(z') \left[ C_F \left( \frac{z}{z'} \mathcal{H}_u(\xi, \xi) - \frac{z(2-z)}{\bar{z}\bar{z}'} \mathcal{H}_u(-\xi, \xi) \right) \right. \\
& + \frac{1}{2N_c} \left( \frac{(z - \bar{z}')^3}{z'\bar{z}'^2\bar{z}|\bar{z}' - z|} \mathcal{H}_u \left( \frac{\xi(z\bar{z}' + \bar{z}\bar{z}')}{1 - z - z'}, \xi \right) - \frac{z}{\bar{z}\bar{z}'^2} \mathcal{H}_u(-\xi, \xi) \right. \\
& + \frac{1}{\bar{z}|z' - z|} \mathcal{H}_u \left( \frac{\xi(z\bar{z}' + z'\bar{z})}{z' - z}, \xi \right) + \frac{z\bar{z}}{z'\bar{z}'^2|z' - z|} \mathcal{H}_u \left( \frac{\xi(z\bar{z}' + z'\bar{z})}{z - z'}, \xi \right) \Big) \\
& \left. + 2 \left( C_F \frac{z(2-z)}{\bar{z}\bar{z}'} + \frac{1}{2N_c} \frac{z}{\bar{z}\bar{z}'} \right) \mathcal{H}_u(-\xi, \xi) \right] \tag{B.16}
\end{aligned}$$

and

$$\begin{aligned}
J_d = & 2C_F \int_{-1}^1 dy \int_0^1 dz' \mathcal{H}_d(y, \xi) \phi_\pi(z') \left[ C_F \left( \frac{\bar{z}(1+z)}{zz'(y - \xi + i\epsilon)} + \frac{\bar{z}}{\bar{z}'(y + \xi - i\epsilon)} \right) \right. \\
& + \frac{1}{2N_c} \left( \frac{\bar{z}}{zz'^2(y - \xi + i\epsilon)} + \frac{(z' - \bar{z})^3}{\bar{z}'z'^2z(y(\bar{z}' - z) - \xi(z\bar{z}' + \bar{z}\bar{z}') + i\epsilon)} \right. \\
& - \frac{1}{z(y(z' - z) - \xi(z\bar{z}' + z'\bar{z}) + i\epsilon)} - \frac{z\bar{z}}{\bar{z}'z'^2(y(z - z') - \xi(z\bar{z}' + z'\bar{z}) + i\epsilon)} \Big) \\
& \left. + (2\pi i) \left( C_F \frac{\bar{z}(1+z)}{zz'} + \frac{1}{2N_c} \frac{\bar{z}}{zz'^2} \right) \delta(y - \xi) \right], \tag{B.17}
\end{aligned}$$

$$\begin{aligned}
-\frac{1}{\pi} \text{Im}(J_d) = & 2C_F \int_0^1 dz' \phi_\pi(z') \left[ C_F \left( \frac{\bar{z}(1+z)}{zz'} \mathcal{H}_d(\xi, \xi) - \frac{\bar{z}}{\bar{z}'} \mathcal{H}_d(-\xi, \xi) \right) \right. \\
& + \frac{1}{2N_c} \left( \frac{(z' - \bar{z})^3}{\bar{z}'z'^2z|\bar{z}' - z'|} \mathcal{H}_d \left( \frac{\xi(z\bar{z}' + \bar{z}\bar{z}')}{1 - z - z'}, \xi \right) + \frac{\bar{z}}{zz'^2} \mathcal{H}_d(\xi, \xi) \right. \\
& - \frac{1}{z|z' - z|} \mathcal{H}_d \left( \frac{\xi(z\bar{z}' + z'\bar{z})}{z' - z}, \xi \right) - \frac{z\bar{z}}{\bar{z}'z'^2|z' - z|} \mathcal{H}_d \left( \frac{\xi(z\bar{z}' + z'\bar{z})}{z - z'}, \xi \right) \Big) \\
& \left. - 2 \left( C_F \frac{\bar{z}(1+z)}{zz'} + \frac{1}{2N_c} \frac{\bar{z}}{zz'^2} \right) \mathcal{H}_d(\xi, \xi) \right]. \tag{B.18}
\end{aligned}$$

The expressions in the last lines of Eqs. (B.15)–(B.18) correspond to the pinch contributions, see text. We do not present explicit expressions for the real parts of the  $u$ - and  $d$ -quark contributions because the corresponding contributions to the dijet cross section are very small.

## References

- [1] V.L. Chernyak and A.R. Zhitnitsky, JETP Lett. **25** (1977) 510; Yad. Fiz. **31** (1980) 1053; V.L. Chernyak, V.G. Serbo and A.R. Zhitnitsky, JETP Lett. **26** (1977) 594; Sov. J. Nucl. Phys. **31** (1980) 552.
- [2] G.P. Lepage and S.J. Brodsky, Phys. Lett. B **87** (1979) 359; Phys. Rev. Lett. **43** (1979) 545,1625 (E); Phys. Rev. D **22** (1980) 2157; S.J. Brodsky, G.P. Lepage and A.A. Zaidi, Phys. Rev. **D23** (1981) 1152.
- [3] A.V. Efremov and A.V. Radyushkin, Phys. Lett. B **94** (1980) 245; Teor. Mat. Fiz. **42** (1980) 147.
- [4] J. C. Collins, L. Frankfurt and M. Strikman, Phys. Rev. D **56** (1997) 2982.
- [5] X. D. Ji, Phys. Rev. D **55** (1997) 7114.
- [6] A. V. Radyushkin, Phys. Lett. B **380** (1996) 417.
- [7] J. C. Collins and A. Freund, Phys. Rev. D **59** (1999) 074009.
- [8] S. J. Brodsky, L. Frankfurt, J. F. Gunion, A. H. Mueller and M. Strikman, Phys. Rev. D **50** (1994) 3134.
- [9] L. D. Landau and I. Ya. Pomeranchuk, J. Exp. Theor. Fiz. **24** (1953) 505; I. Ya. Pomeranchuk and E. L. Feinberg, Dokl. Akad. Nauk Ser. Fiz. **93** (1953) 439; R. J. Glauber, Phys. Rev. **99** (1955) 1515; **100** (1955) 242.
- [10] Z. Vager, R. Naaman and E. P. Kanter, SCIENCE **244** (1989) 426.
- [11] S. F. King, A. Donnachie and J. Randa, Nucl. Phys. B **167** (1980) 98; J. Randa, Phys. Rev. D **22** (1980) 1583.
- [12] G. Bertsch, S. J. Brodsky, A. S. Goldhaber and J. F. Gunion, Phys. Rev. Lett. **47** (1981) 297.
- [13] L. Frankfurt, G. A. Miller and M. Strikman, Phys. Lett. B **304** (1993) 1.
- [14] E. M. Aitala *et al.* [E791 Collaboration], Phys. Rev. Lett. **86** (2001) 4768.
- [15] E. M. Aitala *et al.* [E791 Collaboration], Phys. Rev. Lett. **86** (2001) 4773.
- [16] J. Gronberg *et al.* [CLEO Collaboration], Phys. Rev. D **57** (1998) 33.
- [17] N. N. Nikolaev, W. Schäfer and G. Schwiete, Phys. Rev. D **63** (2001) 014020.
- [18] L. Frankfurt, G. A. Miller and M. Strikman, Found. Phys. **30** (2000) 533 [hep-ph/9907214]; arXiv:hep-ph/0010297.
- [19] V. M. Braun, D. Y. Ivanov, A. Schäfer and L. Szymanowski, Phys. Lett. B **509** (2001) 43.

- [20] V. Chernyak, Phys. Lett. B **516** (2001) 116.
- [21] V. L. Chernyak and A. G. Grozin, Phys. Lett. B **517** (2001) 119.
- [22] D. Müller, D. Robaschik, B. Geyer, F. M. Dittes and J. Horejsi, Fortsch. Phys. **42** (1994) 101 [arXiv:hep-ph/9812448].
- [23] A. V. Radyushkin, Phys. Lett. B **385** (1996) 333; Phys. Rev. D **56** (1997) 5524.
- [24] X. Ji, Phys. Rev. Lett. **78** (1997) 610; J. Phys. **GG24** (1998) 1181.
- [25] A. Szczepaniak, E. M. Henley and S. J. Brodsky, Phys. Lett. B **243** (1990) 287.
- [26] J. Botts and G. Sterman, Nucl. Phys. B **325** (1989) 62; H. n. Li and G. Sterman, Nucl. Phys. B **381** (1992) 129.
- [27] G. T. Bodwin, S. J. Brodsky and G. P. Lepage, Phys. Rev. Lett. **47** (1981) 1799.
- [28] J. C. Collins, D. E. Soper and G. Sterman, Nucl. Phys. B **261** (1985) 104.
- [29] J. C. Collins, D. E. Soper and G. Sterman, Phys. Lett. B **134** (1984) 263.
- [30] S. Catani, M. Ciafaloni and G. Marchesini, Phys. Lett. B **168** (1986) 284; Nucl. Phys. B **264** (1986) 588.
- [31] S. V. Ivanov, G. P. Korchemsky and A. V. Radyushkin, Yad. Fiz. **44** (1986) 230 [Sov. J. Nucl. Phys. **44** (1986) 145];  
G. P. Korchemsky and A. V. Radyushkin, Phys. Lett. B **171** (1986) 459.
- [32] H. Cheng and T. T. Wu, Phys. Rev. **182** (1969) 1852.
- [33] L. N. Lipatov and G. W. Frolov, Sov. Yad. Fiz. **13**, (1971) 588.
- [34] V. L. Chernyak and A. R. Zhitnitsky, Nucl. Phys. B **201** (1982) 492; Phys. Rept. **112** (1984) 173.
- [35] A. Freund and M. F. McDermott, Phys. Rev. D **65** (2002) 074008;  
<http://durpdg.dur.ac.uk/hepdata/dvcs.html>
- [36] A. D. Martin, R. G. Roberts, W. J. Stirling and R. S. Thorne, arXiv:hep-ph/0201127.
- [37] V. N. Gribov and A. A. Migdal, Sov. J. Nucl. Phys. **8** (1969) 583 [Yad. Fiz. **8** (1969) 1002].
- [38] D. Y. Ivanov and L. Szymanowski, Phys. Rev. D **64** (2001) 097506.